Process Biochemistry 92 (2020) 288–302

Contents lists available at ScienceDirect

Process Biochemistry

journal homepage: www.elsevier.com/locate/procbio

In-silico epitope identification and design of Uricase mutein with reduced immunogenicity

Anand Kumar Nelapati[a], Bratin Kumar Das[b], Jagadeesh Babu Ponnan Ettiyappan[a], Debashree Chakraborty[b,*]

[a] Department of Chemical Engineering, National Institute of Technology Karnataka, Surathkal, Mangalore, 575025, India
[b] Biophysical and Computational Chemistry Lab, Department of Chemistry, National Institute of Technology Karnataka, Surathkal, Mangalore, 575025, India

ARTICLE INFO

Keywords:
Uricase
Gout
In-silico mutagenesis
Epitope
Molecular dynamics simulation
Free energy

ABSTRACT

The clinical utilization of Uricase against gout is limited due to the immunogenicity. In the present article, we identified the antigenic determinants of Uricase and reduced their immunogenicity via *in-silico* mutagenesis. Multiple sequence alignment and motif analysis were carried out to identify the conserved residues in evolutionary process. Emini surface accessibility, Parker hydrophilicity, and Karplus & Schulz flexibility methods were employed to predict the linear B-cell epitopes of both *Ag*-Uricase and *Bf*-Uricase. Deimmunization approach identified T-cell epitopes and the hot spot residues. Reduced antigenic probability was obtained in case of T159W, D169C, N264W and Y203D mutations for *Ag*-Uricase, while S139 V, K215W, G216 F and I172 P mutations for *Bf*-Uricase. The binding affinity values of uric acid towards the catalytic pocket of *Ag*-Uricase and *Bf*-Uricase models were found to be -48.71 kcal/mol and -40.93 kcal/mol, respectively. This energy is further stabilized in the mutant model by -6.36 kcal/mol and -1.45 kcal/mol for *Ag*-Uricase and *Bf*-Uricase, respectively. About 100 ns molecular dynamics simulation was performed to evaluate the conformational stability of both native and mutated Uricase. Insights obtained from this study provide guidelines for experimental design of Uricase muteins with reduced antigenicity.

1. Introduction

Heterologous enzymes are believed to be a significant source of biopharmaceuticals due to their substrate specificity [1]. Therapeutic enzymes were therefore used extensively to cure variety of genetic and acquired human diseases by the removal of disease causing metabolites [2,3]. In addition, high catalytic efficiency, high purity, greater affinity, unique selectivity, and good pharmacokinetics properties of these enzymes improve their utility in the current medical arena.

Bacteria are the major sources of therapeutic enzymes. Therapeutic proteins can also be obtained from various biological sources like organs, tissues, animal fluids, and genetically modified organisms and cells [4,5]. During systematic administration of bacterial enzymes, the human body recognizes them as foreign antigen and this leads to secretion of antibodies. Antibody secretion of B-cells is mainly governed by the identification of antigenic epitopes on the surface of bacterial enzymes. Therefore, the use of bacterial enzymes is limited due to their immunogenicity, poor stability and toxicity [6,7]. Moreover, recent uses of therapeutic enzymes are associated with common problems such as high degradation rates or rapid clearance [8].

The most common approach to reduce the antigenicity of bacteria derived biopharmaceuticals was PEGylation [9]. However, polyethylene glycol (PEG) coating of therapeutic protein reduces the efficiency by increasing the protein's size and water absorption properties [10]. In addition, PEGylation can cause PEG specific antibodies to be secreted in the human body [11]. Therefore, the removal of epitopes by protein engineering is known to be a fundamental solution in which antigenic motifs of the therapeutic protein are modified by side directed mutagenesis process to reduce the antigenicity of the protein drug [12–15].

Abbreviations: Ag^N, indicates the hot-spot residue or mutation of *Arthrobactor globiformis*; Bf^N, indicates the hot-spot residue or mutation of *Bacillus fastidious*; CD-4, Cluster of differentiation 4; EMEA, European Medicines Evaluation Agency; HMM, Hidden Markov Model; HLA, Human leukocyte antigen; MEGA, Molecular evolutionary Genetics Analysis; MEME, Multiple EM for Motif Elicitation; MSA, Multiple Sequence Alignment; MHC, Major Histocompatibility Complex; MM/GBSA, Molecular Mechanics/ Generalized Born Surface Area; NCBI, National Center for Biotechnology Information; PSMA, Prostate specific membrane antigen; RMSD, Root Mean Square Deviation; RMSF, Root Mean Square Fluctuation; SAVES, Structure analysis and verification server

* Corresponding author.
E-mail address: debashree@nitk.edu.in (D. Chakraborty).

https://doi.org/10.1016/j.procbio.2020.01.022
Received 7 August 2019; Received in revised form 16 January 2020; Accepted 20 January 2020
Available online 25 January 2020
1359-5113/

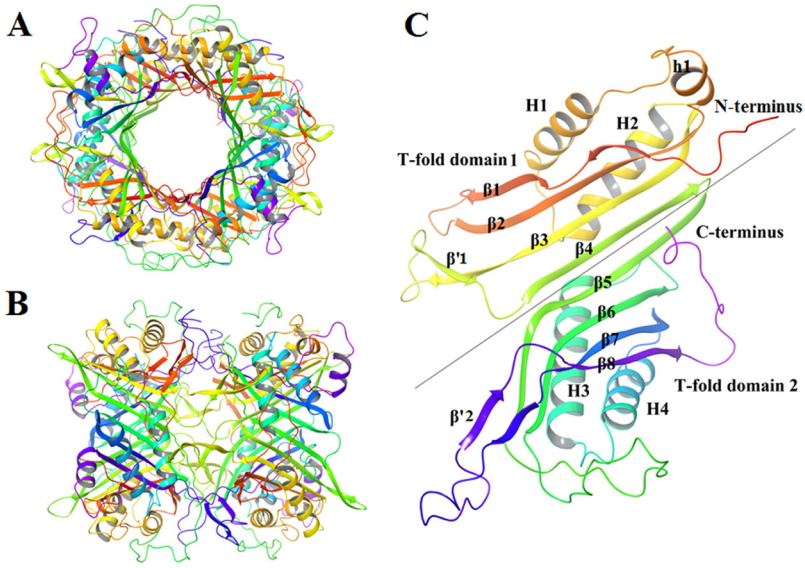

Fig. 1. The complete structure of Uricase (PDB ID: 4R8X). (A) Front view of the tetramer of bacterial Uricase showing the big tunnel at the center of the protein. (B) Side view of Uricase. (C) The monomer of Uricase showing two similar T-domains. β, β', H, h symbols are used to specify the secondary structures like β-sheets and α-helices. (Sourced from: (Ella Czarina Magat Juan et al., 2008).

Uricase or Urate oxidase (EC 1.7.3.3) is a therapeutic enzyme that is involved in the second stage of purine metabolism and is responsible for catalyzing the oxidation of uric acid into water soluble cyclic allantoin, carbon dioxide and hydrogen peroxide that are easily excreted by kidneys [16–19]. Fig. 1 presents the full structure of Uricase (PDB ID: 4R8X). Bacterial Uricase consists of two tetramers composed of four identical subunits. The overall dimension of one tetramer was reported to be 74 × 86 × 76 $Å^3$. Each subunit of Uricase contains 287 amino-acid residues and consists of four α-helices, two one-turn helices, eight long, and two short β-strands [17]. Each monomers of Uricase can be divided into two similar domains known as T-fold domains [20] and each T-fold domains consists of antiparallel *ββαaββ* superfold. A cylindrical tunnel with a rough diameter of 30 Å and length of 80 Å can be found at the center of the Uricase tetramer.

Unlike humans and apes, bacteria, yeast, birds and reptiles have the ability to breakdown uric acid into a more soluble form, allantoin [21–23].The lack of Uricase in the human body results in an increase in the concentration of uric acid in plasma that is much higher compared to most of the other mammals [24]. The imbalance between the rate of production and excretion of uric acid results in exceeding the solubility limit of uric acid in plasma. As a result, uric acid nucleates in the joints and periarticular cavity [25]. The accumulation of uric acid crystals in synovial membrane and synovial fluid is known to be responsible for acute and chronic inflammation. Such medical condition is known as gout flares. Additionally, the deposition of uric acid can also induce tumor lysis syndrome and cardiovascular diseases [26,27].

There have been numerous attempts to treat gout and other hyperuricemia-related diseases through the systematic administration of Uricase extracted from various sources [28]. Non-recombinant form of Uricase (Uricozyme®) from *Aspergillus flavus* was first used for the treatment and prevention of tumor lysis syndrome with hyperuricemia, which is also associated with high risk of renal failure [29–33]. The first recombinant form of Uricase from *Aspergillus flavus* is Rasburicase. Due to its high immunogenicity and short half-life, Rasburicase therapy is stated to be limited [32–37]. Additionally, the therapeutic potential of recombinant Uricase for the treatment of gout is associated with pharmacologic tolerance and potency problems [38,39]. Therefore, it is important to reduce the immunogenicity of Uricase as a protein-drug to cure treatment-resistant gout. The combination of polyethylene glycol with Uricase was reported as the first clinical study to successfully reduce plasma uric acid concentration over 32 h [10,40]. However, due to several limitations of PEGylation of therapeutic enzymes, the identification of hot spot B-cell and T-cell epitopic residues is crucial for the preparation of Uricase mutein which can be easily administered in the human body without immunological effect. Presently, the Uricase used for therapeutic purpose [41–43] are mainly sourced from *Arthrobacter globiformis* and *Bacillus fastidious* due to high specific activity. Therefore, we aim to identify the epitopic regions and decrease the immunogenicity of Uricase from the above mentioned species. The experimental evolution of B-cell and T-cell epitopes of therapeutic proteins are limited because most of the approaches are expensive, time consuming, and labor intensive [44]. Therefore, the widely accepted algorithms and tools of bioinformatics are highly recommended which can reduce cost by predicting B-cell and T-cell epitopes from the amino acid sequence of Uricase [45–47].

In the present study, we aim to identify the linear B-cell, conformational B-cell and MHC-I based T-cell epitopes to reduce the immunogenicity of Uricase sourced from *Arthrobactor globiformis (Ag*-Uricase*),* and *Bacillus fastidious (Bf*-Uricase*)*. Multiple sequence alignment (MSA) was performed to detect the conserved and identical residues of the Uricase from different sources. Motifs and domains of Uricase from various sources were also identified to describe the structural, functional aspects of this protein in the evolutionary process. Emini surface accessibility, Parker hydrophilicity, and Karplus & Schulz flexibility methods were employed to detect the continuous B-cell epitopes and corresponding hot-spot residues. Similarly, deimmunization method was used to identify T-cell epitopes. Next, the hot-spot residues were mutated to reduce the antigenic character of the identified epitopes. Lastly, the impact of mutagenesis on the catalytic activity and the structural stability of Uricase were assessed by molecular docking, free energy calculations and molecular dynamics simulation. To the best of our knowledge, this *in-silico* study to reduce the immunogenicity of bacterial Uricase is presented here for the first time.

2. Methods and computational details

2.1. Uricase sequences retrieval

The amino acid sequences of Uricase were chosen from the following thirteen mass producers, *Drosophila melanogaster* [48], *Oryctolagus cuniculus* [49], *Rattus norvegicus* [50], *Mus musculus* [51], *Cavia porcellus* [52], *Papio hamadryas* [53], *Bacillus fastidious* [54], *Arthrobacter globiformis* [55], *Camelus dromedarius* [56], *Chlamydomonas reinhardtii* [57], *Aspergillus flavus* [58], *Phaseolus vulgaris* [59] and *Cyberlindnera jadinii* [60]. The amino acid sequences of Uricase obtained from the above mentioned prokaryotic and eukaryotic producers were subjected to sequence similarity to understand the conservation and evolutionary relatedness of the taxa. The full length FASTA sequences

of above-mentioned Uricase were collected from the National center for biotechnology information database (NCBI) (https://www.ncbi.nlm.nih.gov/).

2.2. Multiple sequence alignment and phylogenetic comparison

Multiple sequence alignment (MSA) of all the selected amino acid sequences of Uricase from different habitats were performed by ClustalW tool [61] of MEGA (Molecular Evolutionary Genetics Analysis, V-7.0) software [62–64] to identify the conserved residues of Uricase throughout the process of evolution. ClustalW is a widely used matrix-based algorithm that implements progressive alignment methods [65] to align the multiple protein, DNA or RNA sequences from different sources. The parameters used for MSA include gap opening penalty of 10, gap extension penalty of 0.2, gonnect protein weight matrix, and gap distance separation penalty of 5 with no end gap separation. The evolutionary relationship of Uricase was determined by constructing the phylogenetic tree of all thirteen sequences employing maximum parsimony statistical method [66]. The topologies of phylogenetic tree were evaluated by applying 1000 bootstrap replicas [62,64].

2.3. Motif analysis

Multiple EM for Motif Elicitation (MEME) (http://meme-suite.org/tools/meme) is a widely used tool for discovering motifs in a set of related DNA/RNA or protein sequences [67,68]. In proteins, a motif may possibly relate to the enzyme active site or structural unit required for correct folding. Sequence motifs are therefore known as the essential functional units for molecular evolution. The identified motifs and there locations recovered by MEME, elucidate the conserved regions associated with structural and functional properties of Uricase in the evolution process. The starting and ending point of the motifs were displayed as blocks.

Pfam [69], a web-based tool, was used for accurate classification of protein families and domains using HMM (hidden Markov model) (http://pfam.sanger.ac.uk). All the Uricase sequences were submitted in the form of accession numbers to analyze the domain organization associated to Uricase [70,71].

2.4. Antigenic epitopes prediction

Immune epitope database (http://www.iedb.org/) is a standard and organized database with a large collection of experimentally characterized immune epitopes [72]. The amino acid sequences of *Ag*-Uricase and *Bf*-Uricase were retrieved from NCBI and submitted in FASTA format to immune epitope database and analysis resource (IEDB-AR) tool [73] for predicting and analyzing both B-cell and T-cell peptide epitopes.

Surface accessibility, hydrophilicity and mobility are considered critical criteria for assessing the antigenicity of any protein or peptide [74]. Hence, the continuous B-cell epitopes were identified based on Emini surface accessibility, Parker Hydrophilicity, Karplus & Schulz Flexibility prediction methods in the IEDB database [75–78]. Thresholds of 1.00, 1.63 and 0.996 were employed for Surface accessibility, hydrophilicity, and mobility, respectively in the above mentioned methods to determine antigenicity. The FASTA format of *Ag*-Uricase and *Bf*-Uricase sequences were imported to each epitope prediction panel and submitted for predicting B-cell epitopes. All the predicted epitopes where ranked according to their corresponding antigenic scores. The highly immunogenic amino-acid residue inside each epitope peptide was also documented. B-cell linear epitope prediction methods anticipate the immune response according to the characteristics of amino-acid sequence of the antigen using amino acid scales (AASs) and Hidden Markov Models (HMMs) [79–81]. The conformational B-cell epitopes of *Ag*-Uricase and *Bf*-Uricase were identified using Discotope tool (V-2.0) [82]. The server predicts B-cell epitopes based on the spatial information, surface accessibility, and amino acid statistics of discontinuous epitopes identified from the crystal structure of antigen-antibody complex [83]. The 3D-structure of Uricase from both the species were imported to the conformational B-cell epitope prediction panel and a threshold of -3.7 with 17 % sensitivity, and, 95 % specificity was employed.

Next, both *Ag*-Uricase and *Bf*-Uricase protein sequences were screened to identify T-cell epitopes using deimmunization method. The human leukocyte antigen (HLA)-B*5801 allele that is strongly associated with hyperuricemia and gout was chosen for predicting MHC-II based T-cell epitope [84,85].

2.5. In-silico mutagenesis

The crystal structure of *Ag*-Uricase (PDB ID: 2YZB, resolution 1.9 Å) [86] and *Bf*-Uricase (PDB ID: 4R8X, resolution 1.401 Å) [87] was retrieved from protein data bank (PDB) for modeling studies. Both crystal structures of Uricase were prepared using protein preparation workflow [88] in Maestro. The missing hydrogen atoms were added in both structures. It was reported that the functional or active form of Uricase can exists as homotetramer [89]. Therefore, 2YZB was kept in tetrameric form by deleting the extra chains to reduce the size, making it comparable with 4R8X. The Uricase activity is found to be optimal at pH of 9.0 [42,86]. Hence, the protonation state of the amino acid residues of both 2YZB and 4R8X were optimized at a pH of 9.0. The orientations of the hydroxyl group of Asn and Gln residues were also optimized for both crystal structures of Uricase. Next, the structures of both proteins were minimized using OPLS-2005 force field [90,91] with RMSD (protein heavy atoms) convergence criteria of 0.30 Å.

The hot-spot amino acids for *in-silico* mutagenesis were chosen based on the score obtained from B and T cell epitopes prediction of Uricase from both bacterial sources. *In-silico* sight directed mutagenesis (SDM) was performed on both optimized structures of 2YZB and 4R8X, using Pymol software (v 1.6). The obtained mutant proteins were validated using Ramachandran plot and I-MUTANT [92] web-server. The structures were further used for molecular docking to determine the impact of side-directed mutagenesis on their structural and catalytic aspects.

2.6. Ligand preparation

The 3D-structure of the Uric acid was constructed using the builder panel in Maestro (v-11.7.011, Schrödinger, LLC, New York, 2018).The possible ionization state was generated and partial charges were assigned at pH of 9.0 prior to docking. The geometry of the structure was optimized and its energy was minimized using OPLS-2005 force-field [90,91] in Ligprep module (**Schrödinger Release 2018-3**: LigPrep, Schrödinger, LLC, New York, 2018). The resulting structure was considered for further modeling studies.

2.7. Molecular docking

Glide [93] (**Schrödinger Release 2018-3**: Glide, Schrödinger, LLC, New York, 2018) was used to perform docking (Extra Precision mode) of Uric acid at the active sites of both 2YZB and 4R8X. Glide uses a hierarchical array of filters to investigate possible ligand locations at the catalytic pocket of Uricase [94]. The geometry of the Uric acid was kept in flexible mode while the receptor was depicted as rigid. The receptor grid was generated with a partial charge cut-off of 0.25e, and the van- der -walls scaling factor was kept at 1.00. The active site residues of 2YZB i.e. Asn249, Gln223, Leu222, Arg180, Phe163 (Chain A) and Asp68-Ala66 (Chain D) were selected to generate the grid box suitable for accommodating Uric acid, and the grid center was placed at the centroid of the interacting amino acids [86]. Since the catalytic pocket residues of 4R8X are unclear, the amino acids located at the interface of two identical sub-units, such as Phe179, Ala193, Arg196,

Ile244, Gln244, Asn271, Gln299 (Chain C) and Ala68-Asp70 (Chain A) [87,89] were selected to build the grid box. The binding affinity of Uric acid towards both the wild and mutated Uricase was calculated by MM/GBSA method [95]. The detail methodology of MM/GBSA calculation is given in Supplementary S:1. The accuracy of docking was assessed by measuring the RMSD (RMSD = 0.16 Å) between the co-crystal and re-docked position of Uric acid at the catalytic pocket (Fig. S4-A) of Uricase. The binding pose of Uric acid at the active sight of Uricase was further confirmed by molecular dynamics simulation.

2.8. The MD protocol

The native, mutated form of both tetrameric 2YZB and 4R8X (in association with substrate Uric acid) was subjected to atomic molecular dynamic simulation in order to compare their conformational stability under motion. Simulation with all the subsequent calculations were carried out using Desmond [96] package, and Maestro GUI was used for visualization. OPLS-2005 [90,91] force field was used to generate the necessary parameters required for energy minimization and MD simulations of 2YZB and 4R8 X. All four structures of Uricase (including both mutated and normal from the two aforementioned species) were solvated separately in orthorhombic periodic unit with SPC (simple-point charge) water molecules [97]. The resulting systems were neutralized by adding counter ions. In addition, 0.15 M NaCl was added to imitate physiological conditions. Next, the systems were minimized under steepest descent algorithm [98] with a maximum of 2000 iterations until a gradient threshold of 25 kcal/mol/Å is reached.

All the systems of solvated Uricase (mutated and wild structure of both 2YZB and 4R8X) were initially heated up at 300 K for 1 ns and subsequently equilibrated under canonical (NVT) ensemble for 4 ns. Next, the system condition was changed from NVT to isothermal-isobaric (NPT) ensemble at a temperature of 300 K for 5 ns each in order to equilibrate the pressure at 1 atm. During each equilibration step, protein-ligand heavy atoms were restrained. The temperature and pressure of the system were controlled, respectively using Noose-Hoover thermostat [99] and Martyna-Tobias-Klein barostat [100]. Temperature and pressure relaxation time of 2 ps was assigned throughout the equilibration time. Lastly, all protein-ligand complexes were subjected to production simulation for 100 ns with a time step of 2 fs. The restrains on solute heavy atom were removed and allowed to move freely throughout the production run. For long-range electrostatic interactions, smooth Particle Mesh Ewald (PME) method [101] was used with a tolerance of $1 \times e^{-9}$ and for short-range electrostatic interactions, a cut-off radius of 9.0 Å was applied. A multiple time step RESPA (Reversible Reference System Propagator Algorithm) integrator algorithm was employed throughout with a time step of 2 fs for bonded, 2 fs for 'near' bonded, and 6 fs for 'far' non bonded interactions. The trajectories of the solute atoms of all four solvated protein-ligand complexes were retrieved at each 20 ps interval for analyzing the data. The conformational stability of Uricase from both species were assessed by calculating the time evolution of protein backbone RMSD, ligand RMSD, residue wise RMSF and radius of gyration. Change in binding free energy during the course of simulation was also performed using MM/GBSA calculation using Prime [95]. The detailed procedure for calculating the above mentioned quantities are documented in supplementary section-I (Methodology).

3. Results and discussion

3.1. Multiple sequence alignment and phylogenetic analysis

The multiple sequence alignment of thirteen Uricase from different sources was carried out by ClustalW approach. It was reported that the conserved residues are important to explain the structural and functional aspects of Uricase. As shown in Fig. 2 and Table S1, the most of the amino acids are conserved between Uricases from mammalian

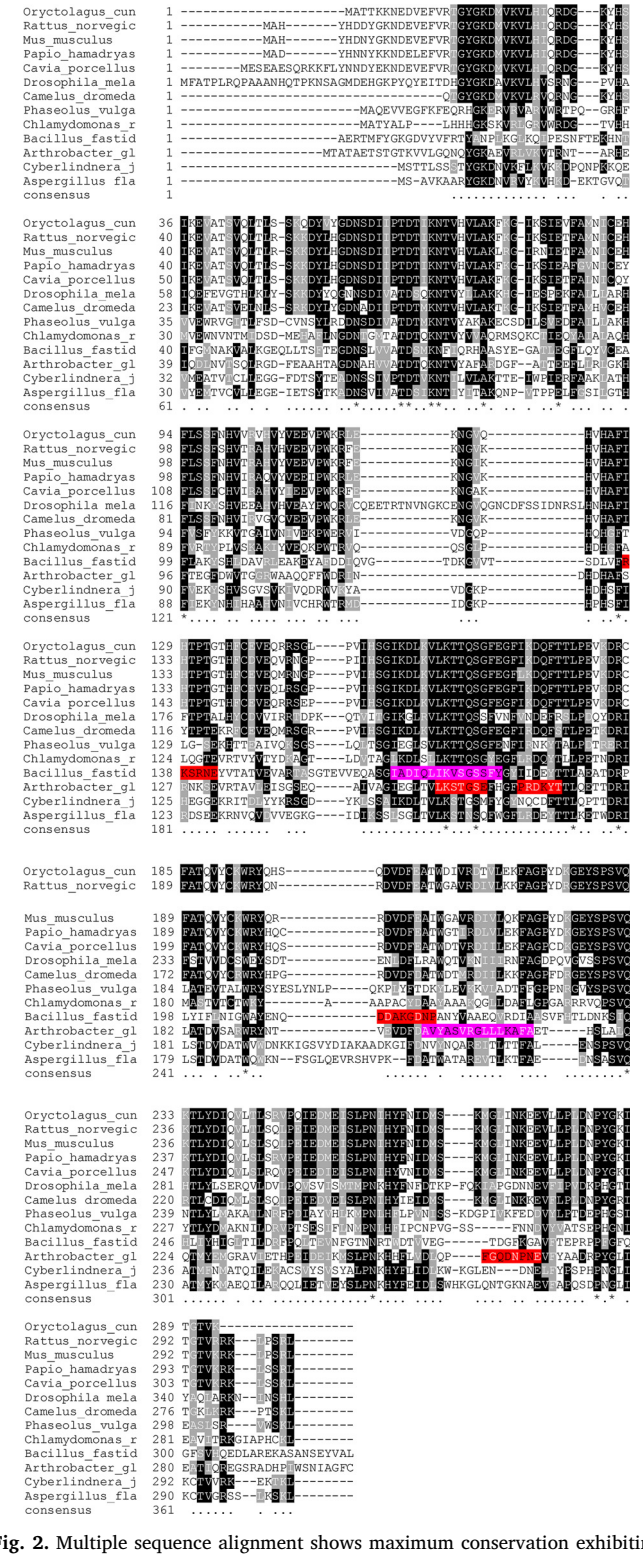

Fig. 2. Multiple sequence alignment shows maximum conservation exhibiting in between 37 and 373 amino acids of Uricase protein sequences from different sources. '*' indicates fully conserved residue and '.' indicates moderately conserved amino acids. The sections are highlighted in red and pink colors are representing B-cell and T-cell epitopic peptides in Uricase sequence. The black color represents identical amino acids, whereas the grey color represents similar amino acids. (For interpretation of the references to colour in this figure legend, the reader is referred to the web version of this article).

sources (78.3–94.6 % sequence identity) compared to those from other sources (21.3–48.2 % sequence identity). For example, the bacterial Uricases from *A.globiformis* and *B.fastidious* showed only 25.26 % identity. In mutagenesis process, it is advised to substitute residues outside the conserved region in order to preserve the structural and functional characteristics of the therapeutic drug [102].

Uricase has a variety of metabolic activities that vary depending on the host organism. A cross-reaction exits between different species of Uricases, possessing similar molecular weight, same cell location, and tissue specificity. This recommends therefore that diverse species of Uricases may have a common evolutionary origin [103,104]. The dendrogram shows that there are two clusters in which one cluster contains Uricase from animal (*R.norvegicus, M.musculus*, *C.porcellus*, *P.hamadryas*, *O.cuniculus*, *C.dromedarius* and *D.melanogaster*) and the second cluster comprises of Uricase from plant (*P.vulgaris*), algal (*C.reinhardtii*), bacterial (*A. globiformis* and *B.fastidious*) and fungal sources (*C.jadinii* and *A.flavus*) (Fig. S1). In the first cluster, it is observed that Uricase from *R.norvegicus*, *M.musculus*, *C.porcellus* and *P.hamadryas* have similarity and identity at the sequence level. In the second cluster, the *P.vulgaris* Uricase show sequence level similarity with the eukaryotic algae *C.reinhardtii*. The fungal source of Uricase from *C.jadinii* and *A.flavus* were observed to be in the same cluster, while the bacterial Uricases from *Arthrobacter globiformis* and *Bacillus fastidious* appeared in a same cluster with similar sequence level. The antigenicity problem was reported to be highly present in therapeutic enzymes from plant source [105]. Therefore, the clinical uses of such plant-derived therapeutic enzymes are limited.

3.2. Motifs conservation

MEME (Motif-based sequence analysis tool) was reported to be based on Bayesian probabilistic model which uses expectation maximization algorithm to obtain the motifs for all the sequences and optimizes the statistical parameters [67]. The maximum number of motifs obtained from Uricase sequences was six and is documented in Table 1.The motifs 2, 3 and 4 are common to all the thirteen Uricases indicating the major function of the enzyme is conserved and these three motifs clearly indicate their potential role in structural and catalytic functional attributes of Uricase. However, Motif 1 and 5 are absent in Uricases from *A.globiformis*, *B.fastidious*, *C.jadinii*, and *A.flavus* and Motif 6 is absent in *D.melanogaster*, *P.vulgaris, C.reinhardtii*, *B.fastidious* and *A.flavus*. The combined block diagram of motifs is displayed in Fig.S2. Other details including motif widths, information about the sequence, and the best possible matches are listed in Table S2.

The Results obtained from Pfam clearly indicate that the monomeric Uricase sequences from various sources have two domain organizations that belong to Uricase family. Each domain consists of 286 amino-acid residues, however, the starting and ending amino acid number varies for each organism. The double domain organization of Uricase monomer indicates the T-fold domains mentioned in Fig. 1.

Table 2
B-cell epitopic scores of *Ag*-Uricase and *Bf*-Uricase. The bold letters are representing the hot spot residues.

Organisms	Method	Peptide	Region	Score
Ag-Uricase	Surface accessibility	PR**D**KYT	167-172	4.904
	Surface accessibility (after-mutation)	PR**C**KYT	167-172	1.64
	Hydrophilicity	GQD**N**PNE	261–267	6.514
	Hydrophilicity (after-mutation)	GQD**W**PNE	261–267	4.086
	Flexibility	LKS**T**GSE	156-162	1.108
	Flexibility (after-mutation)	LKS**W**GSE	156-162	1.029
Bf-Uricase	Surface accessibility	RK**S**RNE	137-142	6.575
	Surface accessibility (after-mutation)	RK**V**RNE	137-142	3.743
	Hydrophilicity	DDA**K**GDN	212-218	7.214
	Hydrophilicity (after-mutation)	DDA**W**GDN	212-218	4.971
	Flexibility	DAK**G**DNP	213-219	1.088
	Flexibility (after-mutation)	DAK**F**DNP	213-219	1.039

3.3. Antigenic epitopes prediction

IEDB epitope database and prediction resource were used to determine the antigenic epitopes of *Ag*-Uricase and *Bf*-Uricase. Continuous sequential regions or various antigenic determinant groups were reported as the major contributors for the formation of antigenic sites or epitopes in a protein [106]. In order to reduce the clinical immunereactiveness of the therapeutic enzyme Uricase, primarily the continuous B-cell epitopes were predicted based on the important antigenic parameters such as Emini surface accessibility, Parker hydrophilicity and Karplus & Schulz flexibility. The majority of the antigenic regions of proteins were reported to have more polar and charged residues rather than hydrophobic residues [15], based on propensity scales for each of the 20 amino acids [107–110]. The predicted B-cell epitope peptides obtained from Emini surface accessibility, Parker hydrophilicity and Karplus & Schulz Flexibility scores of *Ag*-Uricase and *Bf*-Uricase were illustrated in Table S3-6.

In case of *Ag*-Uricase, the B-cell epitopic peptides ^{167}PR**D**KYT^{172}, ^{261}GQD**N**PE^{267} and ^{156}LKS**T**GSE^{162} have the highest surface accessibility score (4.904), parker hydrophilicity score (6.514), Karplus & Schulz flexibility score (1.108), respectively (Table 2), in which the polar residues D169 (Fig. 3-A), N264 (Fig. 3-C) and T159 (Fig. 3-E) made the main contribution to such high score were selected as hot-spot residues for mutagenesis. Similarly, in case of *Bf*-Uricase, the B-cell epitopic peptide ^{137}RK**S**RNE^{142}, ^{212}DDAK**G**DN^{218} and ^{213}DAK**G**DNP^{219} have the highest surface accessibility score (6.575), parker hydrophilicity score (7.214) and Karplus & Schulz flexibility score (1.088), respectively (Table 2) in which the polar residues S139 (Fig. 4-A), K215 (Fig. 4-C) and G216 (Fig. 4-E) were selected as hot-spot residue for

Table 1
Conserved motifs locations for Uricase protein from different source organisms.

S.NO	Organism	Genbank ID	Motif 1	Motif2	Motif 3	Motif 4	Motif 5	Motif 6
1	*Oryctolagus cuniculus*	189303536	7-47	48-76	83-123	147-196	207-236	257-285
2	*Rattus norvegicus*	20127395	11-51	52-80	87-127	151-200	210-239	260-288
3	*Mus musculus*	6678509	11-51	52-80	87-127	151-200	210-239	260-288
4	*Papio hamadryas*	20513624	11-51	52-80	87-127	151-200	211-240	261-289
5	*Cavia porcellus*	884943374	21-61	62-90	97-137	161-210	221-250	271-299
6	*Drosophila melanogaster*	17136576	29-69	70-98	105-145	195-244	255-284	–
7	*Camelus dromedarius*	339716249	–	35-63	70-110	134-183	194-223	244-272
8	*Phaseolus vulgaris*	2809326	–	47-75	83-123	146-195	213-242	–
9	*Chlamydomonas reinhardtii*	11066111	–	42-70	78-118	142-191	201-230	–
10	*Bacillus fastidious*	823631078	–	53-81	88-128	160-209	–	–
11	*Arthrobacter globiformis*	187609193	–	51-79	85-125	144-193	–	248-276
12	*Cyberlindnera jadinii*	1147426164	–	44-72	79-119	143-192	–	260-288
13	*Aspergillus flavus*	137100	–	42-70	77-117	141-190	–	–

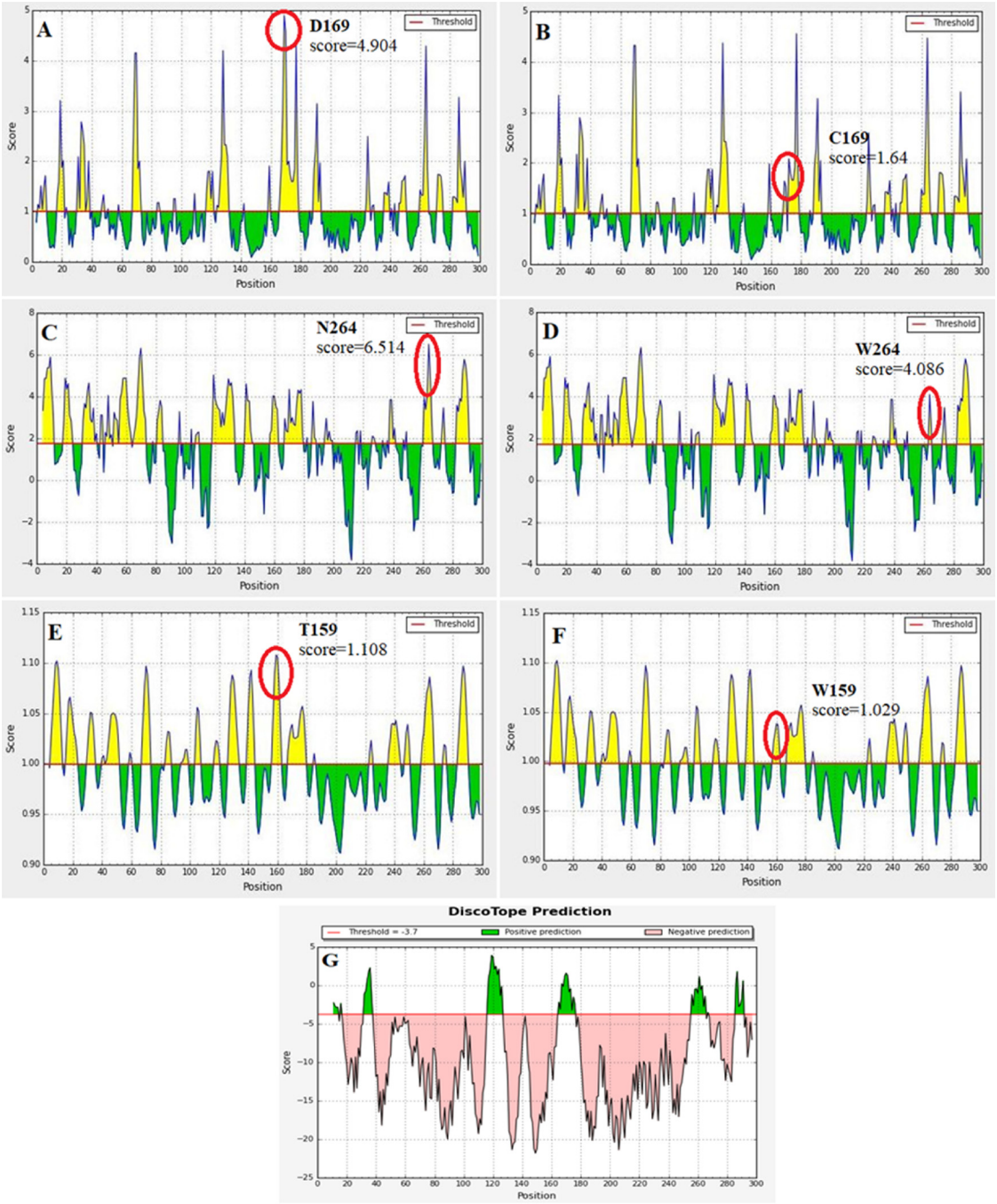

Fig. 3. Graphs represent different regions of the amino acid sequence of Uricase that can act as B-cell epitopes in the case of *Ag*-Uricase **(A)** Emini surface accessibility plot representing maximum antigenicity in *Ag*-Uricase at 167-172. **(B)** Plot presenting the change in surface accessibility score in *Ag*-Uricase at 167-172. **(C)** Parker Hydrophilicity prediction plot presenting maximum antigenicity in *Ag*-Uricase at 261–267. **(D)** The change in hydrophilicity score in *Ag*-Uricase at 261–267. (**E**) Karplus & Schulz Flexibility plot display maximum antigenicity in *Ag*-Uricase at 156-162. **(F)** Plot presenting the change in flexibility score in *Ag*-Uricase at 156-162. **(G)** Graph representing conformational B-cell epitopes from the 3D-structure of *Ag*-Uricase. The selected regions are marked by red circle. (For interpretation of the references to colour in this figure legend, the reader is referred to the web version of this article).

mutagenesis.

In case of *Ag*-Uricase, the conformational B-cell epitopes are found to be overlapped with the peptides predicted as linear B-cell epitope (region ~167-172 and 260–267) indicating the mutations of those two regions are crucial to mask the immunogenicity (Fig.3-G). In contrast, *Bf*-Uricase is found to have very less conformational B-cell epitopes (Fig. 4-G). It can be observed from the highlighted portion of Fig. 2 that all the selected hot spot residues of B-cell epitopes are located at either non-conserved or moderately conserved region indicating that they may have comparatively less significance for preserving the structural and functional characteristics of Uricase [15]. Additionally, all the selected hot-spot residues located at the B-cell epitopic region are polar residues. Therefore, the replacement of these residues with hydrophobic residues was considered as the best way to reduce adverse allergic reaction in human body [111].

T-cell immune responses are induced by identification of T-cell epitopes which are attached to MHC molecules displayed at the surface of antigen presenting cells. T-cell epitope prediction is based on the identification of peptide lengths within an antigen that are capable to stimulate CD4+ T-cells which ultimately elicits the immune response

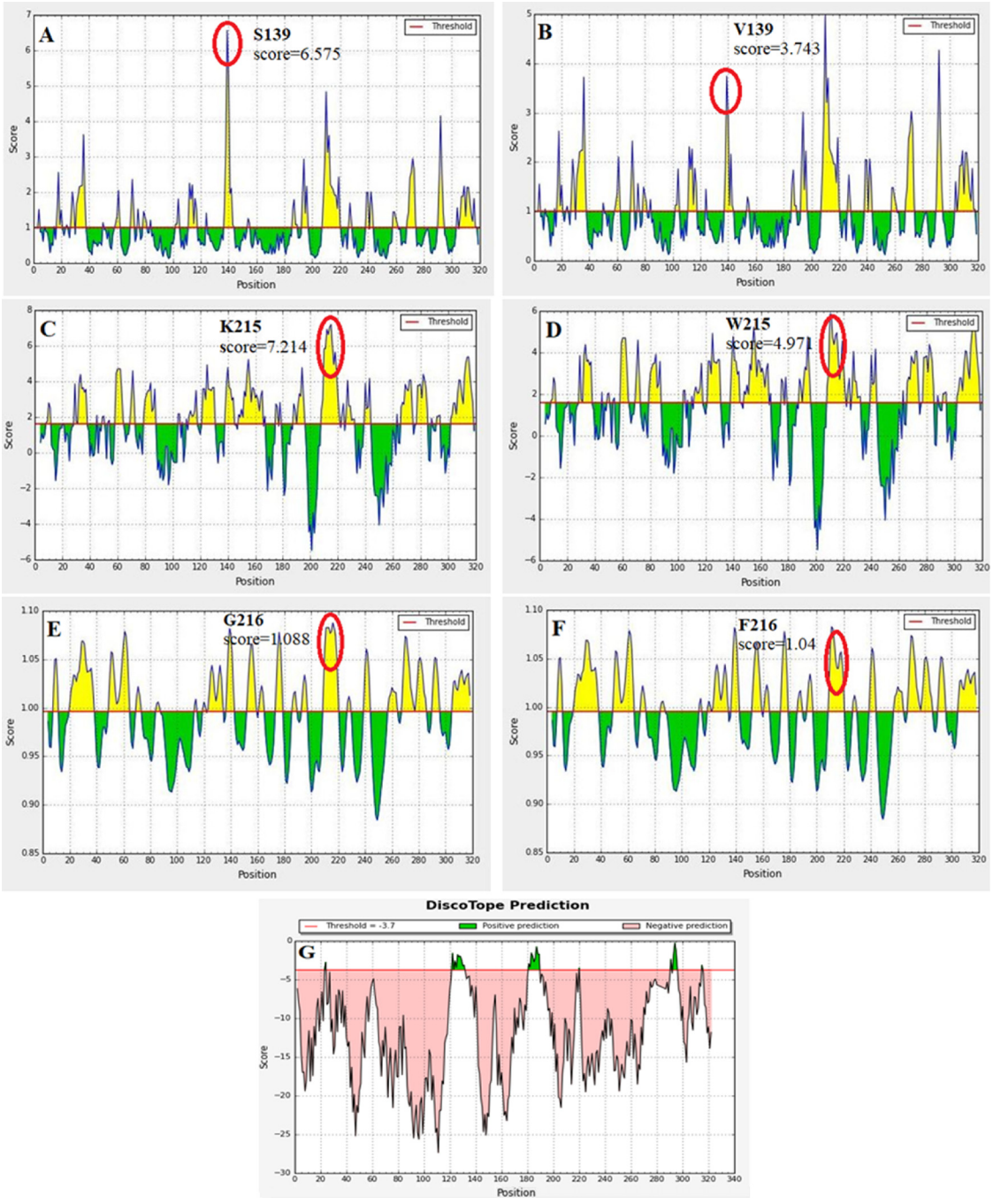

Fig. 4. Graphs represent different regions of the amino acid sequence of Uricase that can act as B-cell epitopes in the case of *Bf*-Uricase **(A)** Emini surface accessibility plot representing maximum antigenicity in *Bf*-Uricase at 137-142. **(B)** Plot presenting the change in surface accessibility score in *Bf*-Uricase at 137-142. **(C)** Parker Hydrophilicity prediction plot presenting maximum antigenicity in *Bf*-Uricase at 212-218. **(D)** Plot presenting the change in hydrophilicity score in *Bf*-Uricase at 212-218. (**E**) Karplus& Schulz Flexibility plot display maximum antigenicity in *Bf*-Uricase at 213-219. (**F**) Plot presenting the change in flexibility score in *Bf*-Uricase at 213-219. (**G**) Representing conformational B-cell epitopes from the 3D-structure of *Bf*-Uricase. The selected regions are marked by red circle. (For interpretation of the references to colour in this figure legend, the reader is referred to the web version of this article).

Table 3
T-cell epitopic scores of *Ag*-Uricase and *Bf*-Uricase. The bold letters are representing the hot spot residues.

S.NO	organism	Peptide	Start position	End position	Median percentile rank
1	*Ag*-Uricase	AV**Y**ASVRGLLLKAFA	201	215	10.78
2	*Bf*-Uricase	IADIQLI**K**VSGSSFY	166	180	8.77

Table 4
T-cell epitopic scores obtained from mutation of all the amino acids with the hot spot residue located at 203 of *Ag*-Uricase and 172 of *Bf*-Uricase. In case of *Ag*-Uricase, Tyr is present in 203 position whereas Ile is present at 172 position in case of *Bf*-Uricase.

S.NO	Amino acids	*Ag*-Uricase	*Bf*-Uricase
1	Native	10.78	8.77
2	Ala	19.685	17.49
3	Cys	19.345	28.97
4	Asp	24.585	30.42
5	Glu	22.9	27.72
6	Phe	8.525	12.25
7	Gly	22.47	35.87
8	His	16.035	27.895
9	Ile	10.84	–
10	Lys	13.555	24.3
11	Leu	12.52	7.325
12	Met	15.245	10.335
13	Asn	21.235	21.675
14	Pro	21.025	51.955
15	Glu	16.465	15.88
16	Arg	14.75	24.715
17	Ser	21.11	23.14
18	Thr	19.15	24.06
19	Val	14.72	12.675
20	Trp	11.105	18.84
21	Tyr	–	16.255

in human body [112]. Deimmunization is a new technology that locates and mutates polypeptide sequences using immunological and molecular biology techniques which helps in reducing protein immunogenicity that does not affect the protein function [113–115]. The success of reduced immunogenicity has been observed in humanized and chimeric antibodies with the removal of potential T-cell epitopes through mutagenesis approach [111,113,116]. A consensus prediction approach is one of the widely used technique for the identification of variable length peptides related to T-cell epitopes [81,117]. Therefore, identifying potential immunogenic T-cell epitopes of *Ag*-Uricase and *Bf*-Uricase are essential for locating the binding sight of MHC-II molecules. The T-cell epitopic peptides obtained in deimmunization analysis is given in Table S7. The lower the median percentile rank, the higher the propensity to act as a epitope [118]. The top scored epitopic peptides are documented in Table 3. The hot-spot residues for the T-cell epitopic peptides are Tyr203, Ile172 for *Ag*-Uricase and *Bf*-Uricase, respectively. The identified hot-spot residues are next subjected to *in-silico* mutagenesis process to obtain less immunogenic candidates of Uricase.

3.4. Residual modification

The hot spot residue of the B-cell, T-cell epitopes of *Ag*-Uricase and *Bf*-Uricase were identified and mutated using Pymol software. The B-cell and T-cell epitopes on the 3D-structure of Uricase from both the sources is shown in Fig. 6 (A,B). In case of *Ag*-Uricase, Asp located at 169 position is found to have high surface accessibility characteristics (Fig. 3-A, Table 2), whereas maximal reduction of antigenic probability is obtained for Ag^{D169C} mutation (Fig. 3-B, Table 2, Table S8). It is evident from Parker hydrophilicity analysis (Fig. 3-C, D, Table 2, Table S8) that Ag^{N264W}mutation causes optimal reduction of immunogenicity of *Ag*-Uricase. The Ag^{T159W}mutation is found to decrease the flexibility characteristics in case of *Ag*-Uricase (Fig. 3-E,F). Similarly, Bf^{S139V} (Fig. 4-A, B, Table S8), Bf^{K215W} (Fig. 4-C, D, Table S8) and Bf^{G216F} (Fig. 4-E, F, Table S8) mutations are found to reduce the surface accessibility and hydrophilicity characteristics of the B-cell epitope of *Bf*-Uricase, respectively. In the case of T-cell epitopes, Ag^{Y203D} mutation gives optimal reduction in immunogenicity for *Ag*-Uricase, whereas, Bf^{I172P} mutation in *Bf*-Uricase is seen as the best result (Table 4, Table S9, and S10). In each subunit, three B-cell (based on Emini surface accessibility, Parker hydrophilicity and Karplus & Schulz flexibility) and one T-cell mutations (based on Deimmunization technique) were carried out. A total of 16 mutations were carried out in each tetrameric form of Uricase sourced from above mentioned species. All four protein models were validated using ΔΔG values (Table S11) and Ramachandran plot (Supplementary Fig. 3, Table S12). All the ΔΔG were found in permissible range. It is evident from Table 1 that mutations are done inside motif 4 and motif 6 which can vary the structural and functional aspects of mutant Uricase models. It can be noticed from the highlighted part of Fig. 2 that the impact for amino acid changes at particular sites in the sequence are less likely to vary the protein structure and function because mutations are mainly done at the non-conserved and moderately conserved portion of the Uricase sequence [102]. Both the wild type and mutated protein models are subjected to molecular docking to have further insights about the functional characteristics of Uricase.

3.5. Molecular docking of uricase

Molecular docking was performed to assess the influence of

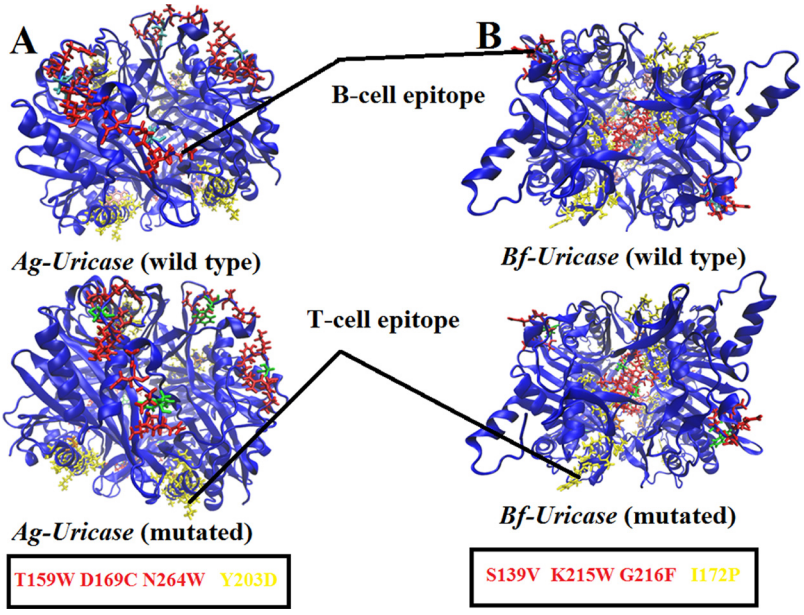

Fig. 5. The locations of B-cell and T-cell epitopes on (A) Ag-Uricase and (B) *Bf*-Uricase. B-cell epitopes are represented in red color and T-cell epitopes are marked in yellow color. The mutated residues are shown in green color. The mutations done in the each monomer of *Ag*-Uricase and *Bf*-Uricase are listed below the enzyme structure. (For interpretation of the references to colour in this figure legend, the reader is referred to the web version of this article).

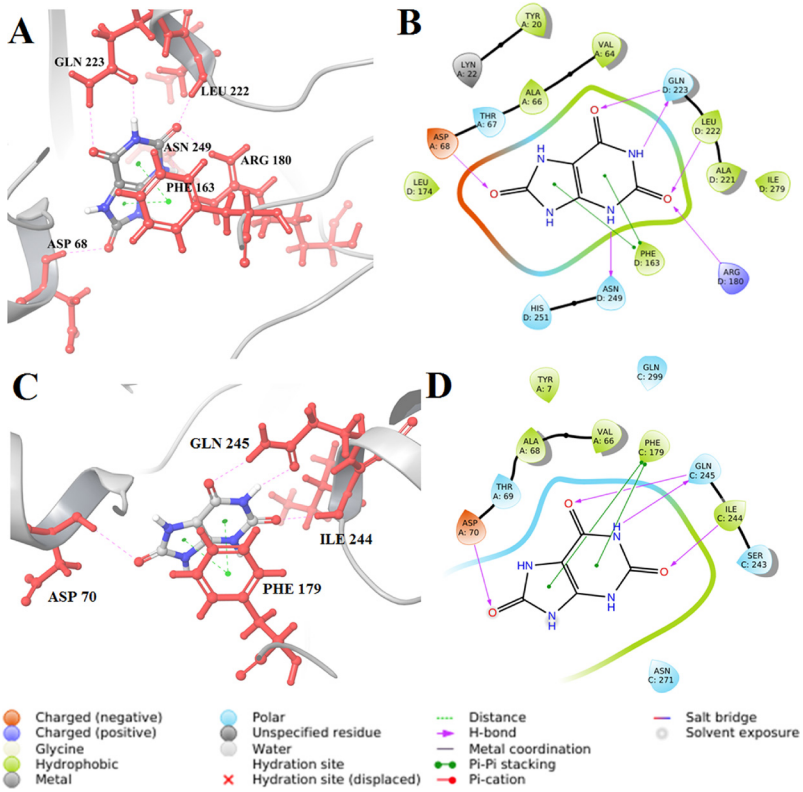

Fig. 6. The docking pose and two dimensional (2D)- ligand interaction diagram of *Ag*-Uricase (A & B) and *Bf*-Uricase (C & D) 4R8 X . The interacting amino acids are represented in red. (For interpretation of the references to colour in this figure legend, the reader is referred to the web version of this article).

Table 5
The docking scores of Uric-acid at the catalytic pocket of wild and mutated Uricase.

S l. No	Organism	Docking score	Binding Energy MM/GBSA (kcal/mol)	Total no of non-bonded interactions	Possible Number of H-bonds
1.	Ag-Uricase (native) (PDB ID: 2YZB)	−8.414	−47.71	7	6
2.	Ag-Uricase (mutated) (PDB ID :2YZB)	−8.570	−48.60	7	6
3.	Bf-Uricase(native) (PDB ID :4R8X)	−5.221	−39.40	5	4
4.	Bf-Uricase(mutated) (PDB ID :4R8X)	−5.389	−41.44	5	4

mutagenesis on the functional aspect of Uricase. The non-bonded interactions between the uric acid and the amino-acid residues at the catalytic pocket of *Ag*-Uricase, *Bf*-Uricase are illustrated in Fig. 5.The binding affinity of docked pose of uric acid towards both the wild type, mutated form of 2YZB (*Ag*-Uricase) and 4R8X (*Bf*-Uricase) are documented in Table 5. The uric acid is found to interact with amino acid residues located at the junction of the identical monomers of 2YZB, indicating a pronounced binding pocket of Uricase (Fig. 6 -A). This binding pocket residues away from the epitopic regions that are located at the surface of Uricase. The uric acid at the catalytic pocket of normal or wild type 2YZB exhibited non bonded interactions with Asp68 of chain A and Phe163, Arg180, Leu222, Gln223 of chain D (Fig. 6-B). The oxygen atom located at the five-membered ring of uric acid is found to accept one hydrogen bond (C═O———−HO-Asp68, hydrogen bond length = 2.39 Å) with the side chain of Asp68. Two hydrogen bonds are formed between the uric acid and Gly223 (NH——O═CGly223 and C═O—HNGly223, hydrogen bond length = 1.94 Å and 2.15 Å, respectively). The nitrogen atom located at the peptide bond between Ala221, Leu222 donates one hydrogen bond to the oxygen atom of uric acid (C═O———HNLeu222, hydrogen bond length 1.83 Å). Another hydrogen bond interaction is found to be present between the oxygen atom of uric acid and side-chain of Arg180 (C═O———NH-Arg180, hydrogen bond length = 2.20 Å). Phe163 is found to exhibit π-π stacking interaction with the heterocyclic rings of uric acid. It is evident from Fig. 6-B that one hydrogen bond is present between the uric acid and the Asn249 (NH———O═C-Asn249, hydrogen bond length = 2.43 Å) which plays an important role in stabilizing the substrate inside the catalytic pocket. It can be observed from Table 5 that the numbers of interactions are unchanged after *in-silico* mutagenesis of 2YZB. However, the binding energy is found to vary after mutation. The binding affinity of uric acid towards wild type 2YZB is found to be -47.7 kcal/mol (Table 5). The per-residue energy contribution of the amino-acid residues towards the binding of uric acid at the catalytic pocket of 2YZB is plotted in Fig. 7-A to understand the protein-ligand association in molecular level. It is clear from Fig. 7-A that the binding affinity of uric acid is mainly dependent on the interaction between Asn249, Gln223, Leu222, Phe163 and Thr67 of 2YZB. Especially, Asn249 (-4.04 kcal/mol), Gln223 (-7.47 kcal/mol) and Phe163 (-5.57 kcal/mol) are the key residues which are responsible for anchoring the ligand at the active site of 2YZB. After the mutation in the

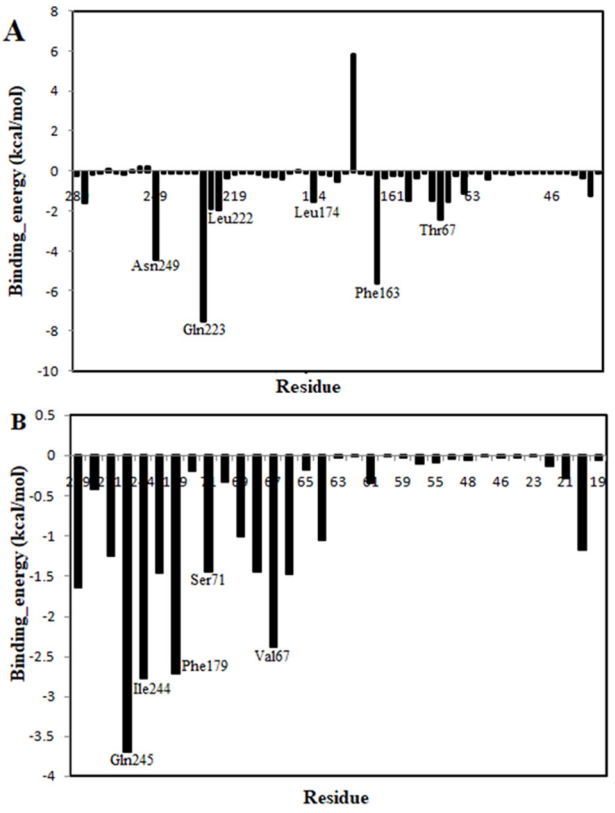

Fig. 7. Residue wise decomposition of binding energy of uric acid towards the catalytic pocket of Uricase. (A) Showing the binding energy decomposition of uric acid in case of *Ag*-Uricase. (B) Showing the residue wise decomposition of uric acid for *Bf*-Uricase.

B-cell and T-cell epitope region of 2YZB, we observed that the binding energy did not changed remarkably (-48.60 kcal/mol). This phenomenon implies that mutation in the backbone of Uricase did not affect the binding of uric acid at the active sight of Uricase and preserved the catalytic activity of the enzyme.

The non-bonded interaction of Uric acid with the catalytic pocket of 4R8X is displayed in Fig. 6-C and D. The Uric acid is located at the interface of chain-C and chain-A of 4R8 X . It is clear from Fig. 6-A, and C that the binding pose of Uric acid in 4R8X is similar with 2YZB. Uric acid is found to have hydrogen bonding interaction with Ile244 (C═O———HN-lle244, hydrogen bond length = 2.02 Å respectively), Gln245 (C═O——NHGln245, C═O——NHGln245, hydrogen bond length 2.21 Å, 2.00 Å, respectively) and exhibit π- π stacking interaction with Phe179 of chain C. Additionally, the oxygen atom located at the five membered ring of uric acid accepts one hydrogen bond from Asp70 of chain A (C═O———NH-Asp70, hydrogen bond length = 2.72 Å). The binding energy of uric acid at the catalytic pocket of wild type 4R8X is found to be -39.40 kcal/mol. The residue wise decomposition of binding energy is illustrated in Fig. 7-B which suggests that Gln245 (-3.704 kcal/mol), Ile244 (-2.783 kcal/mol), Phe179 (-2.720 kcal/mol) and Val67 (-2.377 kcal/mol) play key roles in stabilizing the ligand at the binding pocket of 4R8 ×X. After site directed mutagenesis of 2YZB, the binding energy of Uric acid is found to be -41.44 kcal/mol. It is evident from the binding energy data that catalytic activity of 2YZB did not vary much after *in-silico* mutagenesis process. Thus, it is confirmed from molecular docking and MM/GBSA studies that both the protein model retains the functionality after the reduction of antigenicity.

3.6. Molecular dynamics simulation

100 ns molecular dynamics simulation was performed in each case to confirm the stability of native structure of the protein after *in-silico* mutagenesis. The conformational stability of Uricase was assessed by computing the time evolution of the root mean square deviation (RMSD) and root mean square fluctuation (RMSF) of the MD simulation trajectory. The RMSD of normal protein backbone and mutated protein of both the species are shown in Fig. 8 and compared to study the effect of mutagenesis on the native structure.

In the case of native 2YZB, the RMSD value gradually increased up to 1.82 Å around 1000 frames and became stable with an average value of 1.8 Å (Fig. 8-A). It is clear from the Fig. 8-A that the RMSD of mutated 2YZB increased up to 2.07 Å until 864 frames and similarly became stable like the wild type 2YZB. It is evident from the above mentioned plot that both the native, mutated form of 2YZB displayed less deviation from the starting (t = 0) structure and were found to be stable throughout the simulation time. A RMSD graph between the normal and mutated 4R8X is illustrated in Fig. 8-B. The backbone RMSD of wild type 4R8X increased up to 1.97 Å around 1500 frames of the MD trajectory and then reached to steady state. In contrast, the RMSD value of the mutated 4R8X increased up to 2.24 Å around 1950 frames and stabilized with an average RMSD value of 2.07 Å. The difference between the average RMSDs of both the normal and mutated 4R8X is found to be ~ 0.06 Å at the last phase of the simulation. It is evident from Fig. 8-B that the native as well as the mutated 4R8X are structurally stable. The RMSD of uric acid (ligand) with respect to protein backbone is found to be comparable in the two species both in its native and mutated form (Fig. 8-A, B). This finding confirms the stabilization of the ligand at the catalytic sight after mutation. The root mean square fluctuation (RMSF) measures the residue wise fluctuation during simulation. The RMSF of mutated protein and the normal one was compared to see the fluctuation at the mutated sights (Fig. 8). The average backbone RMSF of native 2YZB is found to be 0.695 Å whereas the mutated 2YZB displayed average RMSF value of 0.693 Å. This indicates that both the native and mutated 2YZB are stable. It is clear from Fig. 8-C that the B-cell epitopic regions 156–162, 167–172, 261–267 of wild type 2YZB have average RMSF values of 0.77 Å, 0.81 Å, and 0.87 Å, respectively. In case of mutated 2YZB, the above mentioned regions have average RMSF values of 0.62 Å, 0.79 Å, and 0.755 Å, respectively, which indicates less fluctuation after mutation. The average RMSF value of the T-cell epitopic region (201–215) of wild type 2YZB is found to be 0.66 Å, whereas the average RMSF value increased to 0.77 Å after mutation. It is clear from the above discussion that fluctuation of the B-cell epitopes reduces after mutation. In contrast, the fluctuation of T-cell RMSF increases after mutation, although negligible. These phenomena indicate that mutated 2YZB has less susceptibility to interact with antibodies and CD4+ cells. Residues 287, 599, 864 are found to be more fluctuated and away from the antigenic region. In case of both native and mutated 4R8X, the average RMSF value is found to be almost similar (around 0.668 Å), indicating stability of both structures (Fig. 8-D). However, the flexibility of mutated region of 4R8X is found to be higher compared to its native type. The average RMSF of T-cell epitope 166–180 displayed higher value (1.94 Å) compared to its native form (0.49 Å). The B-cell epitope region (137–142) showed similar (0.75 Å) fluctuation in mutated from compared to its native form (0.75 Å) (Fig. 8-D). However, the increment of flexibility of antigenic epitope is comparable with its native form. The higher fluctuations are observed at the C-terminal and N-terminal ends of Uricase due to solvent exposure. The time evolution of compactness or the overall size of Uricase was measured by means of radius of gyration (R_g) and is illustrated in Fig. 8-E, F. It is found from Fig. 8-E that both the native and mutated Uricase backbone of 2YZB is found to be stabilized at an average R_g score of 30.3 Å. Similarly, in the case of 4R8X, both the native and mutated Uricase backbone maintained an average R_g value of 31.8 Å (Fig. 8-F). The closeness of R_g value in both the native and mutein Uricase indicates that the compactness of the protein backbone was unchanged after the mutation in antigenic region. The secondary structure contents of both the species are found to

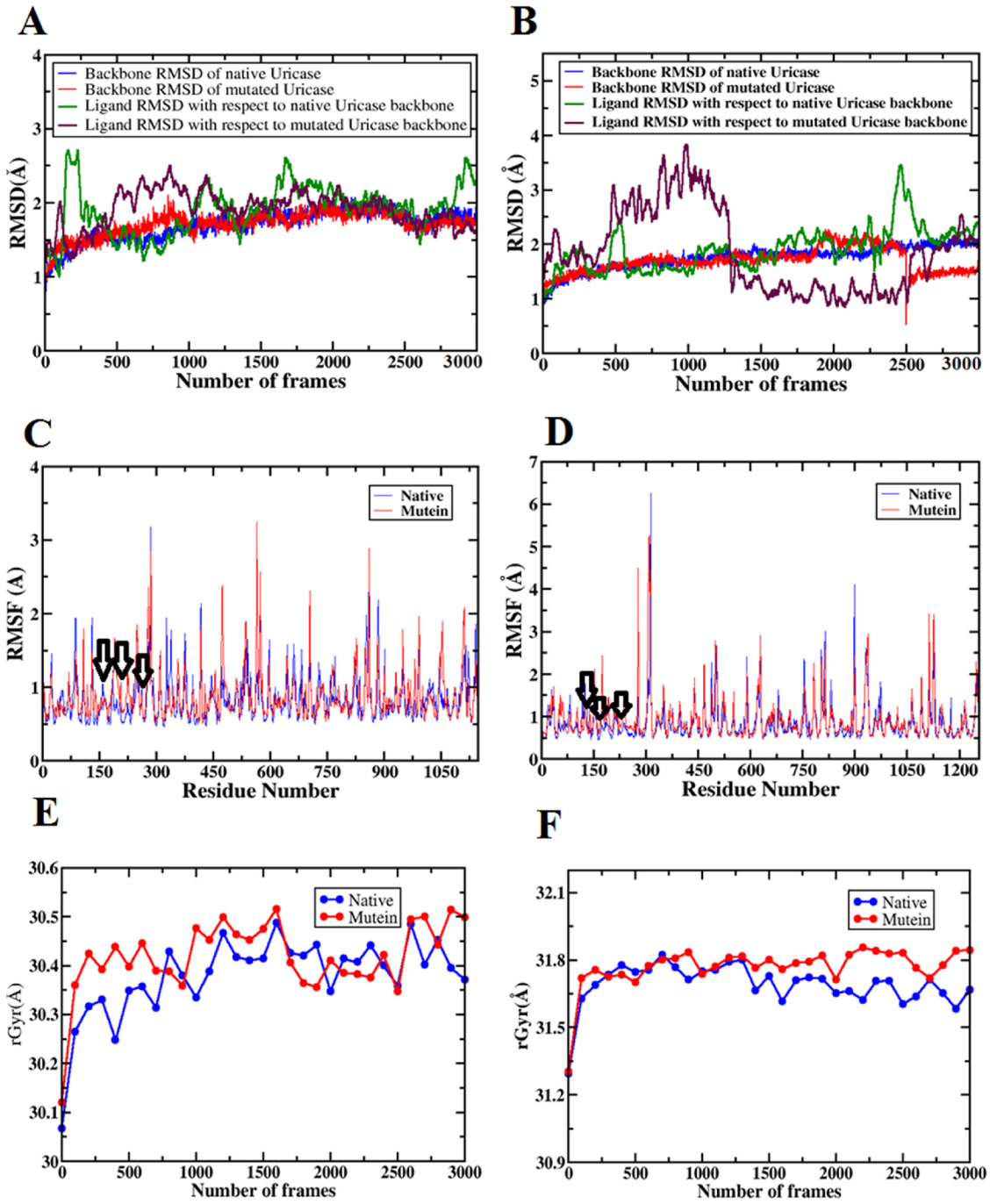

Fig. 8. Comparisons between the backbone RMSDs, RMSFs of the wild type and mutated Uricase. (A) Showing the time evolution of RMSD of *Ag*-Uricase and (B) Showing time evolution of the RMSD of *Bf*-Uricase. (C) Showing the RMSF in case of *Ag*-Uricase. The arrow sign showing the fluctuation in epitopic region (D) Showing RMSF in case of *Bf*-Uricase. The arrow sign showing the fluctuation in epitopic region. (E) The time evolution of the Radius gyration of native (blue) and mutated (red) *Ag*-Uricase. (F) The time evolution of the Radius gyration of native (blue) and mutated (red) *Bf*-Uricase. Blue color represents the native and red color represents the mutein backbone. Green color represents the ligand RMSD in native protein and maroon color represents ligand RMSD in mutated protein. (For interpretation of the references to colour in this figure legend, the reader is referred to the web version of this article).

be similar with their corresponding mutant model (Fig.S5-A, B, C, and D). Hence, the mutations are not responsible for the remarkable secondary structure loss in Uricase.

The time evolution of the binding free energy of uric acid at the active sight of Uricase is presented in Fig. 9-A, B. In both species, the binding free energy is found to be stabilized at the last of the MD trajectory. This further indicates the stability of the ligand at the catalytic pocket of Uricase after mutation. The average binding energy of uric acid at the catalytic pocket of Uricase is found to be -48.71 kcal/mol and -40.93 kcal/mol for 2YZB and 4R8X, respectively. The average binding energy difference (between the mutated and wild type Uricase model) is found to be -6.36 kcal/mol for 2YZB and -1.45 kcal/mol for 4R8 X . During the course of simulation four stable hydrogen bonds are found to be intact among the docking predicted hydrogen bonds between 2YZB and Uric acid. The histograms illustrated in Fig.S6-A reveal that the regions Glu162-Arg180, Leu222-Asn249, and Val64-Asp68 have major interaction with Uric acid during the simulation. After mutation of 2YZB, there was no substantial change in hydrogen

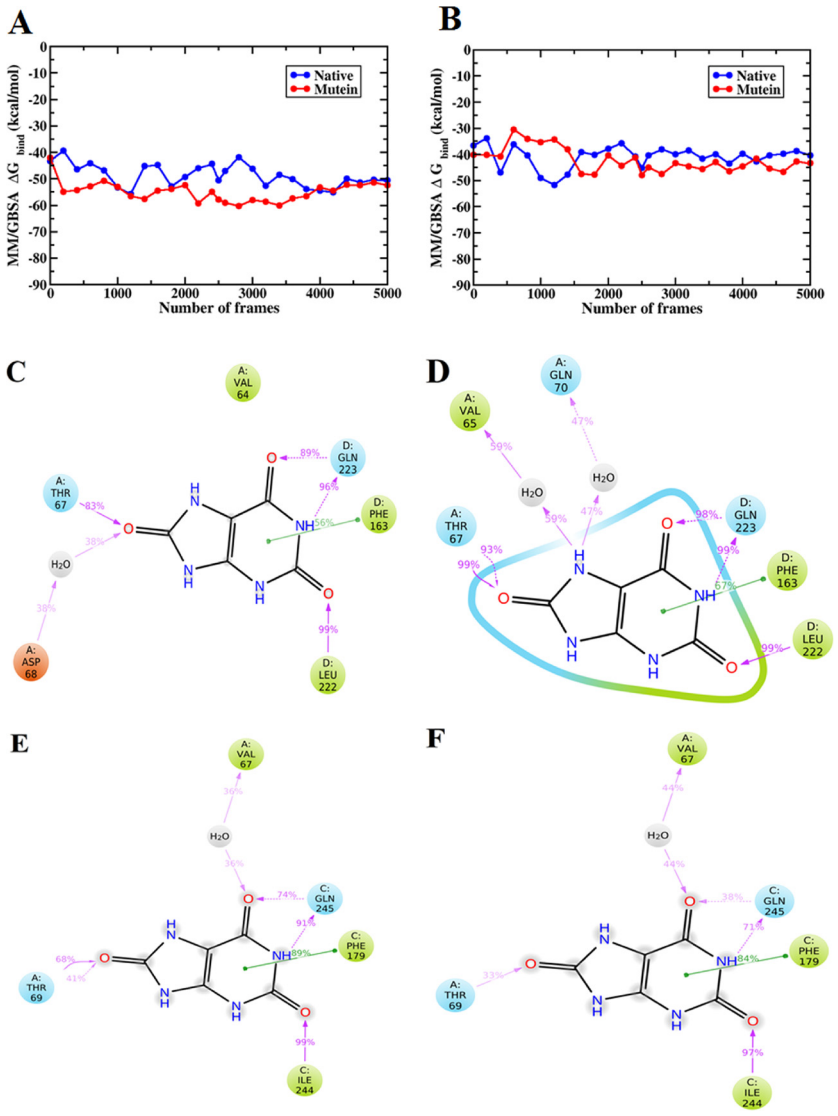

Fig. 9. (A) The change of the binding free energy of uric acid in 2YZB throughout the 100 ns MD simulation. (B) The change of the binding free energy of uric acid in 4R8X throughout the MD simulation. The interaction percentage between the uric acid and the amino-acid residues at the binding pocket of Uricase are represented. (C) & (D) Showing the interaction in case of wild and mutated *Ag*-Uricase. (E) & (F) Showing the interaction in case of wild and mutated *Bf*-Uricase.

bonding interaction profile with the substrate. The interaction of Gln70 with the Uric acid has increased whereas the interaction with Asp68 is found to be decreased (Fig.S6-B). It is clear from Fig. 9-C and Fig.S5-A that Thr67, Leu222, and Gln223 formed hydrogen bonding interaction for 83 %, 99 %, and 96 % of the trajectory. One water mediated hydrogen bonds is observed with Asp68 for 38 % of the simulated trajectory (Fig. 9-**C**). It can be found from Fig.S6-A, B that hydrogen bonding interactions between uric acid and Thr67, Leu222, Gln223 are similar after mutation. One extra water mediated hydrogen bond is present which anchors the ligand with Gln70 for 47 % of the trajectory (Fig. 9-D). The contacts between Uric acid and the interacting amino acid residue in both the wild and mutated 2YZB are found to match with the plot of interaction fractions (Fig.S7-A, B). In case of native 4R8X, the main interacting regions are Val67-Asp70 and Ile244-Asn271 (Fig.S6-C). The non-bonded interactions between binding pocket residues and Uric acid are found to be unchanged after mutation (Fig.S6-D). The NH and O atoms of the six-membered ring of Uric acid formed two hydrogen bonds with Gln245 for 74 % and 91 % of the simulated trajectory (Fig. 9-E). Additionally, Ile244 formed hydrogen bond with uric acid for 99 % of the trajectory. In case of mutated 4R8X, Gln245 formed hydrogen bond with 71 % of the trajectory and Ile244 formed hydrogen bond with 97 % (Fig. 9-F). The contacts between Uric acid and Val67, Thr69, Phe179, Ile244, and Gln245 are found to be similar in both the native and mutated 4R8X (Fig.S7-C, D). Therefore, it is clear from the MD simulation results that the enzyme variants remain stable after mutating immunogenic amino-acids, distributed throughout the protein surface without much change in their catalytic activity.

4. Conclusion

The clinical application of Uricase as an anti-hyperuricemia agent is limited due to antigenicity problem. In order to generate less immune reactive therapeutic drug, *in-silico* mutagenesis of B-cell and T-cell epitope has been proposed. Multiple sequence alignment of thirteen Uricases from different sources was performed to identify the conserved sequence. Out of the six motifs obtained, three were found to be common for all Uricase producers. Motif2, motif3, motif4 are expected to preserve most of the structural and functional aspects of Uricase. In case of *Ag*-Uricase, the epitopic peptide ^{167}PR**D**KYT^{172} was found to be highly surfaced accessible due to the presence of Asp at 169 position. According to Parker hydrophilicity method, the peptide sequence ^{261}GQD**N**PNE^{267} had highest antigenic probability due to the placement

of Asn at 264 position. Peptide sequence ^{156}LKS**T**GSE^{162} was also considered as immunogenic due to the relatively higher flexibility. Similarly, two epitopic peptides ^{137}RK**S**RNE^{142} and ^{212}DDA**K**GDN^{219} were found to influence antibody secretion in the human body for *Bf*-Uricase. The antigenic property of these epitopes was high due to the presence of Ser at 139 and Lys at 215 positions, respectively. Deimmunization studies were carried out to locate the T-cell epitopes for both the species. The epitopic peptides ^{201}AV**Y**ASVRGLLLKAFA^{215} and ^{166}IADIQL**I**KVSGSSFY^{180} were found to have high propensity to activate CD4+ cells for both species. Four hot-spot amino acid residues were identified for each monomer of Uricase. The maximal reduction of immunogenicity was obtained for T159W, D169C, N264W, and Y203D mutations in *Ag*-Uricase and S139V, K215W, G216F, I172P mutations in *Bf*-Uricase. All the amino acid mutations were done in non-conserved and moderately conserved region of Uricase sequence which is less likely to alter the structural and functional characteristics of the therapeutic drug. The stabilization in the binding affinity of uric acid in mutein model of Uricase confirmed that their catalytic activity is unchanged. The MD simulation indicates that both the muteins are stable and they preserve their native like structural characteristics. The insights obtained from the study provide a guideline for experimental development of Uricase drug for treating gout and related diseases.

Declaration of Competing Interest

The authors declare no conflict of interest.

Acknowledgements

Funding from DST, SERB (ECR/2016/000707) is highly acknowledged. BKD is thankful to Department of Science and Technology for providing scholarship. AKN is thankful to National Institute of Technology Karnataka, Surathkal for providing fellowship. We would also like to thank Schrödinger Inc., Department of Chemistry and Department of Chemical Engineering for their constant support.

Appendix A. Supplementary data

Supplementary material related to this article can be found, in the online version, at doi:https://doi.org/10.1016/j.procbio.2020.01.022.

References

[1] C. De Duve, The significance of lysosomes in pathology and medicine, Proc. Inst. Med. Chic. 26 (1966) 73–76.
[2] L.-J. Shen, W.-C. Shen, Drug evaluation: ADI-PEG-20–a PEGylated arginine deiminase for arginine-auxotrophic cancers, Curr. Opin. Mol. Ther. 8 (2006) 240–248.
[3] Y. Tan, M. Xu, R.M. Hoffman, Broad selective efficacy of recombinant methioninase and polyethylene glycol-modified recombinant methioninase on Cancer cells in vitro, Anticancer Res. 30 (2010) 1041–1046 (accessed March 26, 2019), http://ar.iiarjournals.org/content/30/4/1041.
[4] J.D. Valderrama-Rincon, A.C. Fisher, J.H. Merritt, Y.-Y. Fan, C.A. Reading, K. Chhiba, C. Heiss, P. Azadi, M. Aebi, M.P. DeLisa, An engineered eukaryotic protein glycosylation pathway in *Escherichia coli*, Nat. Chem. Biol. 8 (2012) 434–436, https://doi.org/10.1038/nchembio.921.
[5] V. Rodríguez, J.A. Asenjo, B.A. Andrews, Design and implementation of a high yield production system for recombinant expression of peptides, Microb. Cell Fact. 13 (2014) 65, https://doi.org/10.1186/1475-2859-13-65.
[6] C. De Duve, The significance of lysosomes in pathology and medicine, Proc. Inst. Med. Chic. 26 (1966) 73–76.
[7] S.N. Dean, K.B. Turner, I.L. Medintz, S.A. Walper, Targeting and delivery of therapeutic enzymes, Ther. Deliv. 8 (2017) 577–595, https://doi.org/10.4155/tde-2017-0020.
[8] S. Mumtaz, B.K. Bachhawat, Enzyme engineering and its application in lysosomal storage disease, Pure Appl. Chem. 64 (1992) 1055–1060, https://doi.org/10.1351/pac199264081055.
[9] S. Jevševar, M. Kunstelj, V.G. Porekar, PEGylation of therapeutic proteins, Biotechnol. J. 5 (2010) 113–128, https://doi.org/10.1002/biot.200900218.
[10] M.R. Sherman, M.G.P. Saifer, F. Perez-Ruiz, PEG-uricase in the management of treatment-resistant gout and hyperuricemia, Adv. Drug Deliv. Rev. 60 (2008) 59–68, https://doi.org/10.1016/j.addr.2007.06.011.
[11] J.K. Armstrong, G. Hempel, S. Koling, L.S. Chan, T. Fisher, H.J. Meiselman, G. Garratty, Antibody against poly(ethylene glycol) adversely affects PEG-asparaginase therapy in acute lymphoblastic leukemia patients, Cancer. 110 (2007) 103–111, https://doi.org/10.1002/cncr.22739.
[12] F.A. Harding, A.D. Liu, M. Stickler, O.J. Razo, R. Chin, N. Faravashi, W. Viola, T. Graycar, V.P. Yeung, W. Aehle, D. Meijer, S. Wong, M.H. Rashid, A.M. Valdes, V. Schellenberger, A β-lactamase with reduced immunogenicity for the targeted delivery of chemotherapeutics using antibody-directed enzyme prodrug therapy, Mol. Cancer Ther. 4 (2005) 1791–1800, https://doi.org/10.1158/1535-7163.MCT-05-0189.
[13] A. Mayer, S.K. Sharma, B. Tolner, N.P. Minton, D. Purdy, P. Amlot, G. Tharakan, R.H.J. Begent, K.A. Chester, Modifying an immunogenic epitope on a therapeutic protein: a step towards an improved system for antibody-directed enzyme prodrug therapy (ADEPT), Br. J. Cancer 90 (2004) 2402–2410, https://doi.org/10.1038/sj.bjc.6601888.
[14] L.N. Ramya, K.K. Pulicherla, Studies on deimmunization of antileukaemic L-Asparaginase to have reduced clinical immunogenicity–An *in silico* approach, Pathol. Oncol. Res. 21 (2015) 909–920, https://doi.org/10.1007/s12253-015-9912-0.
[15] M. Zarei, N. Nezafat, M.R. Rahbar, M. Negahdaripour, S. Sabetian, M.H. Morowvat, Y. Ghasemi, Decreasing the immunogenicity of arginine deiminase enzyme via structure-based computational analysis, J. Biomol. Struct. Dyn. 37 (2019) 523–536, https://doi.org/10.1080/07391102.2018.1431151.
[16] I. Ramazzina, C. Folli, A. Secchi, R. Berni, R. Percudani, Completing the uric acid degradation pathway through phylogenetic comparison of whole genomes, Nat. Chem. Biol. 2 (2006) 144–148, https://doi.org/10.1038/nchembio768.
[17] E.C.M. Juan, M.M. Hoque, S. Shimizu, M.T. Hossain, T. Yamamoto, S. Imamura, K. Suzuki, M. Tsunoda, H. Amano, T. Sekiguchi, A. Takénaka, Structures of *Arthrobacter globiformis* urate oxidase-ligand complexes, Acta Crystallogr. D Biol. Crystallogr. 64 (2008) 815–822, https://doi.org/10.1107/S0907444908013590.
[18] T.R. Merriman, N. Dalbeth, The genetic basis of hyperuricaemia and gout, Joint Bone Spine 78 (2011) 35–40, https://doi.org/10.1016/j.jbspin.2010.02.027.
[19] A.K. Nelapati, J. PonnanEttiyappan, Computational analysis of therapeutic enzyme uricase from different source organisms, Curr. Proteomics 16 (2019), https://doi.org/10.2174/1570164616666190617165107.
[20] N. Colloc'h, M.E. Hajji, B. Bachet, G. L'Hermite, M. Schiltz, T. Prangé, B. Castro, J.-P. Mornon, Crystal Structure of the protein drug urate oxidase-inhibitor complex at 2.05 Å resolution, Nat. Struct. Biol. 4 (1997) 947, https://doi.org/10.1038/nsb1197-947.
[21] J. Keilin, The biological significance of uric acid and guanine excretion, Biol. Rev. 34 (1959) 265–294, https://doi.org/10.1111/j.1469-185X.1959.tb01308.x.
[22] G.D. Vogels, C. Van der Drift, Degradation of purines and pyrimidines by microorganisms, Bacteriol. Rev. 40 (1976) 403–468.
[23] R.M. Hafez, T.M. Abdel-Rahman, R.M. Naguib, Uric acid in plants and microorganisms: biological applications and genetics - A review, J. Adv. Res. 8 (2017) 475–486, https://doi.org/10.1016/j.jare.2017.05.003.
[24] X.W. Wu, D.M. Muzny, C.C. Lee, C.T. Caskey, Two independent mutational events in the loss of urate oxidase during hominoid evolution, J. Mol. Evol. 34 (1992) 78–84.
[25] L.K. Stamp, J.L. O'Donnell, P.T. Chapman, Emerging therapies in the long-term management of hyperuricaemia and gout, Intern. Med. J. 37 (2007) 258–266, https://doi.org/10.1111/j.1445-5994.2007.01315.x.
[26] O. Bessmertny, L.M. Robitaille, M.S. Cairo, Rasburicase: a new approach for preventing and/or treating tumor lysis syndrome, Curr. Pharm. Des. 11 (2005) 4177–4185.
[27] G. Del Toro, E. Morris, M.S. Cairo, Tumor lysis syndrome: pathophysiology, definition, and alternative treatment approaches, Clin. Adv. Hematol. Oncol. 3 (2005) 54–61.
[28] M. London, P.B. Hudson, Uricolytic activity of purified uricase in two human beings, Science. 125 (1957) 937–938, https://doi.org/10.1126/science.125.3254.937.
[29] P. Laboureur, C. Langlois, [Urate oxidase of *Aspergillus flavus*, I. Isolation, purification, properties], Bull. Soc. Chim. Biol. 50 (1968) 811–825.
[30] P. Kissel, G. Mauuary, R. Royer, P. Toussain, Letter: Treatment of malignant haemopathies and urate oxidase, Lancet. 1 (1975) 229.
[31] G. Masera, M. Jankovic, M.G. Zurlo, A. Locasciulli, M.R. Rossi, C. Uderzo, M. Recchia, Urate-oxidase prophylaxis of uric acid-induced renal damage in childhood leukemia, J. Pediatr. 100 (1982) 152–155, https://doi.org/10.1016/S0022-3476(82)80259-X.
[32] G. Nuki, Uricase therapy of gout, Gout & Other Crystal Arthropathies, Elsevier, 2012, pp. 174–186, https://doi.org/10.1016/B978-1-4377-2864-4.10014-4.
[33] R.P. Garay, M.R. El-Gewely, J.-P. Labaune, P. Richette, Therapeutic perspectives on uricases for gout, Joint Bone Spine 79 (2012) 237–242, https://doi.org/10.1016/j.jbspin.2012.01.004.
[34] A. Bayol, J. Capdevielle, P. Malazzi, A. Buzy, M. Claude Bonnet, N. Colloc'h, J.-P. Mornon, D. Loyaux, P. Ferrara, Modification of a reactive cysteine explains differences between rasburicase and Uricozyme, a natural *Aspergillus flavus* uricase, Biotechnol. Appl. Biochem. 36 (2002) 21–31 https://doi.org/10.1042/.
[35] B. Coiffier, N. Mounier, S. Bologna, C. Fermé, H. Tilly, A. Sonet, B. Christian, O. Casasnovas, E. Jourdan, K. Belhadj, R. Herbrecht, Efficacy and tolerability of pegloticase for the treatment of chronic gout in patients refractory to conventional treatment: two randomized controlled trials, J. Clin. Oncol. 21 (2003) 4402–4406, https://doi.org/10.1200/JCO.2003.04.115.
[36] Q.-Y. Tan, J.-Q. Zhang, N. Wang, H. Yang, X. Li, H.-R. Xiong, J.-Y. Wu, C.-J. Zhao, H. Wang, H.-F. Yin, Improved biological properties and hypouricemic effects of uricase from *Candida utilis* loaded in novel alkaline enzymosomes, Int. J.

Nanomedicine 7 (2012) 3929–3938, https://doi.org/10.2147/IJN.S33835.
[37] P. Szczurek, N. Mosiichuk, J. Woliński, T. Yatsenko, D. Grujic, L. Lozinska, M. Pieszka, E. Święch, S.G. Pierzynowski, K. Goncharova, Oral uricase eliminates blood uric acid in the hyperuricemic pig model, PLoS One 12 (2017) e0179195, , https://doi.org/10.1371/journal.pone.0179195.
[38] H.S.B. Baraf, A.K. Matsumoto, A.N. Maroli, R.W. Waltrip, Resolution of gouty tophi after twelve weeks of pegloticase treatment, Arthritis Rheum. 58 (2008) 3632–3634, https://doi.org/10.1002/art.23993.
[39] A. Guttmann, S. Krasnokutsky, M.H. Pillinger, A. Berhanu, Pegloticase in gout treatment - safety issues, latest evidence and clinical considerations, Ther. Adv. Drug Saf. 8 (2017) 379–388, https://doi.org/10.1177/2042098617727714.
[40] S. Davis, Y.K. Park, A. Abuchowski, F.F. Davis, Hypouricaemic effect of poly-ethyleneglycol modified urate oxidase, Lancet. 2 (1981) 281–283.
[41] A. Punnappuzha, J. PonnanEttiyappan, R.S. Nishith, S. Hadigal, P.G. Pai, Synthesis and characterization of polysialic acid–Uricase conjugates for the treatment of Hyperuricemia, Int. J. Pept. Res. Ther. 20 (2014) 465–472, https://doi.org/10.1007/s10989-014-9411-2.
[42] Q. Tan, J. Zhang, N. Wang, X. Li, H. Xiong, Y. Teng, D. He, J. Wu, C. Zhao, H. Yin, L. Zhang, Uricase from *Bacillus fastidious* loaded in alkaline enzymosomes: enhanced biochemical and pharmacological characteristics in hypouricemic rats, Eur. J. Pharm. Biopharm. 82 (2012) 43–48, https://doi.org/10.1016/j.ejpb.2012.06.002.
[43] Y. Zhao, L. Zhao, G. Yang, J. Tao, Y. Bu, F. Liao, Characterization of uricase from *Bacillus fastidious* A.T.C.C. 26904 and its application to serum uric acid assay by a patented kinetic uricase method, Biotechnol. Appl. Biochem. 45 (2006) 75, https://doi.org/10.1042/BA20060028.
[44] L. Potocnakova, M. Bhide, L.B. Pulzova, An introduction to B-Cell Epitope Mapping and In Silico Epitope PredictionJ Immunolepitope mapping and *in silico* epitope prediction, J. Immunol. Res. 2016 (2016), https://doi.org/10.1155/2016/6760830.
[45] A.S. Kolaskar, P.C. Tongaonkar, A semi-empirical method for prediction of antigenic determinants on protein antigens, FEBS Lett. 276 (1990) 172–174.
[46] S. Saha, G.P.S. Raghava, Prediction of continuous B-cell epitopes in an antigen using recurrent neural network, Proteins. 65 (2006) 40–48, https://doi.org/10.1002/prot.21078.
[47] H. Singh, H.R. Ansari, G.P.S. Raghava, Improved method for linear B-Cell epitope prediction using antigen's primary sequence, PLoS One 8 (2013) e62216, , https://doi.org/10.1371/journal.pone.0062216.
[48] T.B. Friedman, A.P. Barker, Purification and partial characterization of urate oxidase from Drosophila melanogaster, Insect Biochem. 12 (1982) 563–570, https://doi.org/10.1016/0020-1790(82)90026-9.
[49] M. Oda, Y. Satta, O. Takenaka, N. Takahata, Loss of urate oxidase activity in hominoids and its evolutionary implications, Mol. Biol. Evol. 19 (2002) 640–653, https://doi.org/10.1093/oxfordjournals.molbev.a004123.
[50] M. Ito, M. Nakamura, H. Ogawa, S. Kato, Y. Takagi, Structural analysis of the gene encoding rat uricase, Genomics. 11 (1991) 905–913, https://doi.org/10.1016/0888-7543(91)90013-5.
[51] Y. Lee, B.C. Park, D.H. Lee, K.-H. Bae, S. Cho, C.H. Lee, J.S. Lee, P.K. Myung, S.G. Park, Mouse transthyretin-related protein is a hydrolase which degrades 5-hydroxyisourate, the end product of the uricase reaction, Mol. Cells 22 (2006) 141–145.
[52] S. Fujiwara, H. Ohashi, T. Noguchi, Comparison of intraperoxisomal localization form and properties of amphibian (Rana catesbeiana) uricase with those of other animal uricases, Comp. Biochem. Physiol. Part B Comp. Biochem. 86 (1987) 23–26, https://doi.org/10.1016/0305-0491(87)90169-6.
[53] R. Xiong, S. Umar, J. Chen, Process for production of recombinant baboon uricase in *Escherichia coli* Rosetta (DE3), Biotechnol. Biotechnol. Equip. 27 (2013) 4141–4144, https://doi.org/10.5504/BBEQ.2013.0064.
[54] Y. Zhao, L. Zhao, G. Yang, J. Tao, Y. Bu, F. Liao, Characterization of uricase from *Bacillus fastidious* A.T.C.C. 26904 and its application to serum uric acid assay by a patented kinetic uricase method, Biotechnol. Appl. Biochem. 45 (2006) 75, https://doi.org/10.1042/BA20060028.
[55] K. Suzuki, S.-I. Sakasegawa, H. Misaki, M. Sugiyama, Molecular cloning and expression of uricase gene from *Arthrobacter globiformis* in *Escherichia coli* and characterization of the gene product, J. Biosci. Bioeng. 98 (2004) 153–158, https://doi.org/10.1016/S1389-1723(04)00259-2.
[56] A.M. Osman, A.D. Corso, P.L. Ipata, U. Mura, Liver uricase in *Camelus dromedarius*: purification and properties, Comp. Biochem. Physiol. Part B Comp. Biochem. 94 (1989) 469–474, https://doi.org/10.1016/0305-0491(89)90183-1.
[57] J.M. Alamillo, J. Cárdenas, M. Pineda, Purification and molecular properties of urate oxidase from *Chlamydomonas reinhardtii*, Biochimica et Biophysica Acta (BBA) - Protein Structure and Molecular Enzymology 1076 (1991) 203–208, https://doi.org/10.1016/0167-4838(91)90267-4.
[58] P. Leplatois, B. Le Douarin, G. Loison, High-level production of a peroxisomal enzyme: *aspergillus flavus* uricase accumulates intracellularly and is active in *Saccharomyces cerevisiae*, Gene. 122 (1992) 139–145, https://doi.org/10.1016/0378-1119(92)90041-M.
[59] K. Papadopoulou, A. Roussis, H. Kuin, P. Katinakis, Expression pattern of uricase II gene during root nodule development in *Phaseolus vulgaris*, Experientia. 51 (1995) 90–94.
[60] V. Adámek, M. Suchová, K. Demnerová, B. Králová, I. Fořt, P. Morava, Fermentation of *Candida utilis* for uricase production, J. Ind. Microbiol. 6 (1990) 85–89, https://doi.org/10.1007/BF01576427.
[61] J.D. Thompson, D.G. Higgins, T.J. Gibson, W. Clustal, Improving the sensitivity of progressive multiple sequence alignment through sequence weighting, position-specific gap penalties and weight matrix choice, Nucleic Acids Res. 22 (1994) 4673–4680.
[62] S. Kumar, G. Stecher, K. Tamura, MEGA7: Molecular Evolutionary Genetics Analysis Version 7.0 for Bigger Datasets, Mol. Biol. Evol. 33 (2016) 1870–1874, https://doi.org/10.1093/molbev/msw054.
[63] S. Kumar, K. Tamura, I.B. Jakobsen, M. Nei, MEGA2: molecular evolutionary genetics analysis software, Bioinformatics. 17 (2001) 1244–1245, https://doi.org/10.1093/bioinformatics/17.12.1244.
[64] S. Kumar, M. Nei, J. Dudley, K. Tamura, MEGA: a biologist-centric software for evolutionary analysis of DNA and protein sequences, Brief. Bioinformatics 9 (2008) 299–306, https://doi.org/10.1093/bib/bbn017.
[65] M. Chatzou, C. Magis, J.-M. Chang, C. Kemena, G. Bussotti, I. Erb, C. Notredame, Multiple sequence alignment modeling: methods and applications, Brief. Bioinformatics 17 (2016) 1009–1023, https://doi.org/10.1093/bib/bbv099.
[66] D.W. Mount, Maximum parsimony method for phylogenetic prediction, Cold Spring Harb. Protoc. 2008 (2008), https://doi.org/10.1101/pdb.top32 pdb.top32-pdb.top32..
[67] T.L. Bailey, M. Boden, F.A. Buske, M. Frith, C.E. Grant, L. Clementi, J. Ren, W.W. Li, W.S. Noble, M.E.M.E. SUITE, Tools for motif discovery and searching, Nucleic Acids Res. 37 (2009) 202–208, https://doi.org/10.1093/nar/gkp335.
[68] T.L. Bailey, J. Johnson, C.E. Grant, W.S. Noble, The MEME suite, Nucleic Acids Res. 43 (2015) 39–49, https://doi.org/10.1093/nar/gkv416.
[69] S. El-Gebali, J. Mistry, A. Bateman, S.R. Eddy, A. Luciani, S.C. Potter, M. Qureshi, L.J. Richardson, G.A. Salazar, A. Smart, E.L.L. Sonnhammer, L. Hirsh, L. Paladin, D. Piovesan, S.C.E. Tosatto, R.D. Finn, The Pfam protein families database in 2019, Nucleic Acids Res. 47 (2019) D427–D432, https://doi.org/10.1093/nar/gky995.
[70] S.J. Sammut, R.D. Finn, A. Bateman, Pfam 10 years on: 10,000 families and still growing, Brief. Bioinformatics 9 (2008) 210–219, https://doi.org/10.1093/bib/bbn010.
[71] R.D. Finn, A. Bateman, J. Clements, P. Coggill, R.Y. Eberhardt, S.R. Eddy, A. Heger, K. Hetherington, L. Holm, J. Mistry, E.L.L. Sonnhammer, J. Tate, M. Punta, Pfam: the protein families database, Nucleic Acids Res. 42 (2014) 222–230, https://doi.org/10.1093/nar/gkt1223.
[72] Y. Kim, J. Ponomarenko, Z. Zhu, D. Tamang, P. Wang, J. Greenbaum, C. Lundegaard, A. Sette, O. Lund, P.E. Bourne, M. Nielsen, B. Peters, Immune epitope database analysis resource, Nucleic Acids Res. 40 (2012) 525–530, https://doi.org/10.1093/nar/gks438.
[73] Q. Zhang, P. Wang, Y. Kim, P. Haste-Andersen, J. Beaver, P.E. Bourne, H.-H. Bui, S. Buus, S. Frankild, J. Greenbaum, O. Lund, C. Lundegaard, M. Nielsen, J. Ponomarenko, A. Sette, Z. Zhu, B. Peters, Immune epitope database analysis resource (IEDB-AR), Nucleic Acids Res. 36 (2008) 513–518, https://doi.org/10.1093/nar/gkn254.
[74] J.M.R. Parker, D. Guo, R.S. Hodges, New hydrophilicity scale derived from high-performance liquid chromatography peptide retention data: correlation of predicted surface residues with antigenicity and x-ray-derived accessible sites, Biochemistry. 25 (1986) 5425–5432, https://doi.org/10.1021/bi00367a013.
[75] E.A. Emini, J.V. Hughes, D.S. Perlow, J. Boger, Induction of hepatitis A virus-neutralizing antibody by a virus-specific synthetic peptide, J. Virol. 55 (1985) 836–839.
[76] P.A. Karplus, G.E. Schulz, Prediction of chain flexibility in proteins, Naturwissenschaften. 72 (1985) 212–213, https://doi.org/10.1007/BF01195768.
[77] J.E.P. Larsen, O. Lund, M. Nielsen, Improved method for predicting linear B-cell epitopes, Immunome Res. 2 (2006) 2, https://doi.org/10.1186/1745-7580-2-2.
[78] J.M.R. Parker, D. Guo, R.S. Hodges, New hydrophilicity scale derived from high-performance liquid chromatography peptide retention data: correlation of predicted surface residues with antigenicity and x-ray-derived accessible sites, Biochemistry. 25 (1986) 5425–5432, https://doi.org/10.1021/bi00367a013.
[79] K. Yu, N. Petrovsky, C. Schönbach, J.Y.L. Koh, V. Brusic, Methods for prediction of peptide binding to MHC molecules: a comparative study, Mol. Med. 8 (2002) 137–148.
[80] B. Peters, H.-H. Bui, S. Frankild, M. Nielson, C. Lundegaard, E. Kostem, D. Basch, K. Lamberth, M. Harndahl, W. Fleri, S.S. Wilson, J. Sidney, O. Lund, S. Buus, A. Sette, A community resource benchmarking predictions of peptide binding to MHC-I molecules, PLoS Comput. Biol. 2 (2006) e65, https://doi.org/10.1371/journal.pcbi.0020065.
[81] M. Moutaftsi, B. Peters, V. Pasquetto, D.C. Tscharke, J. Sidney, H.-H. Bui, H. Grey, A. Sette, A consensus epitope prediction approach identifies the breadth of murine T(CD8+)-cell responses to vaccinia virus, Nat. Biotechnol. 24 (2006) 817–819, https://doi.org/10.1038/nbt1215.
[82] J.V. Kringelum, C. Lundegaard, O. Lund, M. Nielsen, Reliable B cell epitope predictions: impacts of method development and improved benchmarking, PLoS Comput. Biol. 8 (2012) e1002829, , https://doi.org/10.1371/journal.pcbi.1002829.
[83] P. Haste Andersen, M. Nielsen, O. Lund, Prediction of residues in discontinuous B-cell epitopes using protein 3D structures, Protein Sci. 15 (2006) 2558–2567, https://doi.org/10.1110/ps.062405906.
[84] D.-J. Park, J.-H. Kang, J.-W. Lee, K.-E. Lee, L. Wen, T.-J. Kim, Y.-W. Park, S.-H. Park, S.-S. Lee, Cost-effectiveness analysis of HLA-B5801 genotyping in the treatment of gout patients with chronic renal insufficiency in Korea, Arthritis Care Res (Hoboken). 67 (2015) 280–287, https://doi.org/10.1002/acr.22409.
[85] T.-M. Ko, C.-Y. Tsai, S.-Y. Chen, K.-S. Chen, K.-H. Yu, C.-S. Chu, C.-M. Huang, C.-R. Wang, C.-T. Weng, C.-L. Yu, S.-C. Hsieh, J.-C. Tsai, W.-T. Lai, W.-C. Tsai, G.-D. Yin, T.-T. Ou, K.-H. Cheng, J.-H. Yen, T.-L. Liou, T.-H. Lin, D.-Y. Chen, P.-J. Hsiao, M.-Y. Weng, Y.-M. Chen, C.-H. Chen, M.-F. Liu, H.-W. Yen, J.-J. Lee, M.-C. Kuo, C.-C. Wu, S.-Y. Hung, S.-F. Luo, Y.-H. Yang, H.-P. Chuang, Y.-C. Chou, H.-T. Liao, C.-W. Wang, C.-L. Huang, C.-S. Chang, M.-T.M. Lee, P. Chen, C.-S. Wong, C.-H. Chen, J.-Y. Wu, Y.-T. Chen, C.-Y. Shen, Use of HLA-B*58:01 genotyping to

prevent allopurinol induced severe cutaneous adverse reactions in Taiwan: national prospective cohort study, BMJ (2015) h4848, https://doi.org/10.1136/bmj.h4848.
[86] E.C.M. Juan, M.M. Hoque, S. Shimizu, M.T. Hossain, T. Yamamoto, S. Imamura, K. Suzuki, M. Tsunoda, H. Amano, T. Sekiguchi, A. Takénaka, Structures of *Arthrobacter globiformis* urate oxidase–ligand complexes, Acta Cryst D. 64 (2008) 815–822, https://doi.org/10.1107/S0907444908013590.
[87] J. Feng, L. Wang, H. Liu, X. Yang, L. Liu, Y. Xie, M. Liu, Y. Zhao, X. Li, D. Wang, C.-G. Zhan, F. Liao, Crystal structure of *Bacillus fastidious* uricase reveals an unexpected folding of the C-terminus residues crucial for thermostability under physiological conditions, Appl. Microbiol. Biotechnol. 99 (2015) 7973–7986, https://doi.org/10.1007/s00253-015-6520-6.
[88] G.M. Sastry, M. Adzhigirey, T. Day, R. Annabhimoju, W. Sherman, Protein and ligand preparation: parameters, protocols, and influence on virtual screening enrichments, J. Comput, Aided Mol. Des. 27 (2013) 221–234, https://doi.org/10.1007/s10822-013-9644-8.
[89] J.T. Kratzer, M.A. Lanaspa, M.N. Murphy, C. Cicerchi, C.L. Graves, P.A. Tipton, E.A. Ortlund, R.J. Johnson, E.A. Gaucher, Evolutionary history and metabolic insights of ancient mammalian uricases, Proc. Natl. Acad. Sci. U.S.A. 111 (2014) 3763, https://doi.org/10.1073/pnas.1320393111.
[90] D. Shivakumar, J. Williams, Y. Wu, W. Damm, J. Shelley, W. Sherman, Prediction of absolute solvation free energies using molecular dynamics free energy perturbation and the OPLS force field, J. Chem. Theory Comput. 6 (2010) 1509–1519, https://doi.org/10.1021/ct900587b.
[91] *William L. Jorgensen, David S. Maxwell, J. Tirado-Rives, Development and Testing of the OPLS All-Atom Force Field on Conformational Energetics and Properties of Organic Liquids, (1996), https://doi.org/10.1021/ja9621760.
[92] E. Capriotti, P. Fariselli, R. Casadio, I-Mutant2.0: predicting stability changes upon mutation from the protein sequence or structure, Nucleic Acids Res. 33 (2005) 306–310, https://doi.org/10.1093/nar/gki375.
[93] R.A. Friesner, R.B. Murphy, M.P. Repasky, L.L. Frye, J.R. Greenwood, T.A. Halgren, P.C. Sanschagrin, D.T. Mainz, Extra precision glide: docking and scoring incorporating a model of hydrophobic enclosure for protein-ligand complexes, J. Med. Chem. 49 (2006) 6177–6196, https://doi.org/10.1021/jm051256o.
[94] R.A. Friesner, J.L. Banks, R.B. Murphy, T.A. Halgren, J.J. Klicic, D.T. Mainz, M.P. Repasky, E.H. Knoll, M. Shelley, J.K. Perry, D.E. Shaw, P. Francis, P.S. Shenkin, Glide: a new approach for rapid, accurate docking and scoring. 1. Method and assessment of docking accuracy, J. Med. Chem. 47 (2004) 1739–1749, https://doi.org/10.1021/jm0306430.
[95] S. Genheden, U. Ryde, The MM/PBSA and MM/GBSA methods to estimate ligand-binding affinities, Expert Opin. Drug Discov. 10 (2015) 449–461, https://doi.org/10.1517/17460441.2015.1032936.
[96] K.J. Bowers, E. Chow, H. Xu, R.O. Dror, M.P. Eastwood, B.A. Gregersen, J.L. Klepeis, I. Kolossvary, M.A. Moraes, F.D. Sacerdoti, J.K. Salmon, Y. Shan, D.E. Shaw, Scalable Algorithms for Molecular Dynamics Simulations on Commodity Clusters, in: Proceedings of the 2006 ACM/IEEE Conference on Supercomputing, ACM, New York, NY, USA, 2006, https://doi.org/10.1145/1188455.1188544.
[97] W.L. Jorgensen, J. Chandrasekhar, J.D. Madura, R.W. Impey, M.L. Klein, Comparison of simple potential functions for simulating liquid water, J. Chem. Phys. 79 (1983) 926–935, https://doi.org/10.1063/1.445869.
[98] F.W. Averill, G.S. Painter, Steepest-descent determination of occupation numbers and energy minimization in the local-density approximation, Phys. Rev. B 46 (1992) 2498–2502, https://doi.org/10.1103/PhysRevB.46.2498.
[99] G.J. Martyna, M.L. Klein, M. Tuckerman, Nosé–hoover chains: the canonical ensemble via continuous dynamics, J. Chem. Phys. 97 (1992) 2635–2643, https://doi.org/10.1063/1.463940.
[100] G.J. Martyna, D.J. Tobias, M.L. Klein, Constant pressure molecular dynamics algorithms, J. Chem. Phys. 101 (1994) 4177–4189, https://doi.org/10.1063/1.467468.
[101] U. Essmann, L. Perera, M.L. Berkowitz, T. Darden, H. Lee, L.G. Pedersen, A smooth particle mesh Ewald method, J. Chem. Phys. 103 (1995) 8577–8593, https://doi.org/10.1063/1.470117.
[102] J. Sun, T. Xu, S. Wang, G. Li, D. Wu, Z. Cao, Does Difference Exist Between Epitope and Non-epitope Residues? (2011), p. 11.
[103] A. Varela-Echavarría, R. Montes de Oca-Luna, H.A. Barrera-Saldaña, Uricase protein sequences: conserved during vertebrate evolution but absent in humans, FASEB J. 2 (1988) 3092–3096, https://doi.org/10.1096/fasebj.2.15.3192041.
[104] M. Oda, Y. Satta, O. Takenaka, N. Takahata, Loss of urate oxidase activity in hominoids and its evolutionary implications, Mol. Biol. Evol. 19 (2002) 640–653, https://doi.org/10.1093/oxfordjournals.molbev.a004123.
[105] F. Sánchez, F. Campos, J. Padilla, J.M. Bonneville, C. Enríquez, D. Caput, Purification, cDNA Cloning, and Developmental Expression of the Nodule-Specific Uricase from *Phaseolus vulgaris L*, Plant Physiol. 84 (1987) 1143–1147.
[106] L.N. Ramya, K.K. Pulicherla, Studies on deimmunization of antileukaemic L-Asparaginase to have reduced clinical immunogenicity- an *in silico*approach, Pathol. Oncol. Res. 21 (2015) 909–920, https://doi.org/10.1007/s12253-015-9912-0.
[107] H.B. Bull, K. Breese, Surface tension of amino acid solutions: a hydrophobicity scale of the amino acid residues, Arch. Biochem. Biophys. 161 (1974) 665–670.
[108] M.A. Roseman, Hydrophilicity of polar amino acid side-chains is markedly reduced by flanking peptide bonds, J. Mol. Biol. 200 (1988) 513–522.
[109] L. Malherbe, T-cell epitope mapping, annals of allergy, Asthma & Immunology. 103 (2009) 76–79, https://doi.org/10.1016/S1081-1206(10)60147-0.
[110] T.A. Ahmad, A.E. Eweida, L.H. El-Sayed, T-cell epitope mapping for the design of powerful vaccines, Vaccine Rep. 6 (2016) 13–22, https://doi.org/10.1016/j.vacrep.2016.07.002.
[111] N.H. Bander, M.I. Milowsky, D.M. Nanus, L. Kostakoglu, S. Vallabhajosula, S.J. Goldsmith, Phase I trial of 177lutetium-labeled J591, a monoclonal antibody to prostate-specific membrane antigen, in patients with androgen-independent prostate cancer, J. Clin. Oncol. 23 (2005) 4591–4601, https://doi.org/10.1200/JCO.2005.05.160.
[112] R.K.S. Ahmed, M.J. Maeurer, T-cell epitope mapping, in: M. Schutkowski, U. Reineke (Eds.), Epitope Mapping Protocols, Humana Press, Totowa, NJ, 2009, pp. 427–438, , https://doi.org/10.1007/978-1-59745-450-6_31.
[113] D.J. Macfarlane, R.C. Smart, W.W. Tsui, M. Gerometta, P.R. Eisenberg, A.M. Scott, Safety, pharmacokinetic and dosimetry evaluation of the proposed thrombus imaging agent 99mTc-DI-DD-3B6/22-80B3 Fab′, Eur. J. Nucl. Med. Mol. Imaging 33 (2006) 648–656, https://doi.org/10.1007/s00259-005-0025-y.
[114] T.D. Jones, L.J. Crompton, F.J. Carr, M.P. Baker, Deimmunization of monoclonal antibodies, Methods Mol. Biol. 525 (2009) 405–423, https://doi.org/10.1007/978-1-59745-554-1_21 xiv.
[115] J.R. Cantor, T.H. Yoo, A. Dixit, B.L. Iverson, T.G. Forsthuber, G. Georgiou, Therapeutic enzyme deimmunization by combinatorial T-cell epitope removal using neutral drift, Proc. Natl. Acad. Sci. U.S.A. 108 (2011) 1272–1277, https://doi.org/10.1073/pnas.1014739108.
[116] R.G.E. Holgate, M.P. Baker, Circumventing immunogenicity in the development of therapeutic antibodies, IDrugs. 12 (2009) 233–237.
[117] Z.B. Moola, M.D. Scawen, T. Atkinson, D.J. Nicholls, *Erwinia chrysanthemi* L-asparaginase: epitope mapping and production of antigenically modified enzymes, Biochem. J. 302 (Pt 3) (1994) 921–927.
[118] S.K. Dhanda, A. Grifoni, J. Pham, K. Vaughan, J. Sidney, B. Peters, A. Sette, Development of a strategy and computational application to select candidate protein analogues with reduced HLA binding and immunogenicity, Immunology 153 (2018) 118–132, https://doi.org/10.1111/imm.12816.